6
The influence of source location, shape and plunge in recovery of magnetisation direction from magnetic field data

C.A. Foss

ABSTRACT

Parametric magnetic field inversion requires simultaneous solution of multiple source values. The estimated values for magnetisation (strength and direction) are subject to error in compensation for corresponding errors in the spatial parameters and in this chapter I investigate systematic relationships between error in magnetisation and spatial parameters. Vertical location and extent of a magnetisation does not substantially influence its estimated direction. There is, however, considerable trade-off between horizontal position and magnetisation direction. For well-defined magnetic fields at moderate to large distances from the magnetisation we should expect errors in magnetisation direction associated with mis-positioning of the magnetisation to be of the order of 5° or less. Controls on the horizontal distribution of magnetisation by plunge are the most problematic single-parameter trade-off for magnetisation direction, giving rise to uncertainties in magnetisation direction of up to 7°. Errors in estimated magnetisation direction increase with proximity to the magnetisation where shape factors become more prominent, with increasing complexity of the distribution of magnetisation, and with increasing challenges of isolating the magnetic field of the magnetisation.

6.1 INTRODUCTION

Many magnetic field analyses and inversions ignore the complexity arising from magnetisation direction. Those that seek to address it (Roest and Pilkington 1993; Fedi *et al.* 1994; Schmidt and Clark 1998; Paine *et al.* 2001; Dransfield *et al.* 2003; Phillips 2005; Dannemiller and Li 2006; Foss 2006; Lelièvre and Oldenburg 2009; Foss and McKenzie 2011; Clark 2014; Pratt *et al.* 2014; Fullagar and Pears 2015) either act to include magnetisation direction directly in analysis or inversion or to partially mitigate its effect. However, there has been no systematic evaluation of the capabilities and limitations with which analysis or inversion of magnetic field data can succeed without prior knowledge of its direction. The only analytic proof that magnetisation direction can be reliably recovered from magnetic field data is by Helbig (1963) derived specifically for dipole analysis of a magnetisation at a pre-defined horizontal location. For inversion of distal field data of a compact magnetisation the key challenge is to correctly separate the field to be analysed from any other superimposed field variations. Closer to the magnetisation, field variations include expressions of the shape and plunge of the magnetisation that disrupt reliable estimation of its direction.

A magnetic field variation generated by a discrete subsurface magnetisation depends on its horizontal position, depth, size, shape, orientation, magnetisation intensity and direction. Many magnetic field measurements have substantial further complication that they include contributions from multiple sources that cannot be uniquely separated. I investigate the fortunate but still challenging case that an isolated magnetisation

produces a field variation sufficiently well defined that it can be confidently isolated from the background field. The analyses are restricted to compact magnetisations that have maximum extent no greater than twice the closest approach of the magnetic field measurements and computations. Bodies with a single large vertical axis (pipes) or with at least two large axes (sheets) require separate analysis. Parametric inversion is well suited to analysis of the sensitivities of the relationships between magnetisations and their external magnetic fields. It allows investigation of the influence of individual model parameters while keeping others fixed, and also supports investigation of how two or more parameters interact. These investigations illustrate fundamental relationships between a magnetisation and its magnetic field that are relevant to parametric and voxel inversion and any related analysis. The findings of this synthetic data study are well confirmed in a study of aeromagnetic data acquired near Rylstone, New South Wales.

6.2 INFLUENCE OF SOURCE LOCATION ALONE

In magnetic field inversion there is strong trade-off between estimation of horizontal source position and magnetisation direction. To investigate this relationship, I first attempt to recover magnetisation direction for a displaced equidimensional source with no complication of shape or orientation. Figure 6.1 shows a series of dipole (homogeneous spherical magnetisation) centre-points in north–south and east–west traverses over images of TMI (Fig. 6.1A) and total gradient of TMI (Fig. 6.1B) computed for an induced dipole magnetisation in a geomagnetic field of inclination −60°. It is difficult to accurately select the horizontal centre of magnetisation from the TMI image. A reduced to pole (RTP) transform can be used to centre the magnetic field anomaly over the magnetisation but only if the magnetisation direction is already known. Alternatively, the total gradient transform (also known as the analytic signal or modulus of the analytic signal) can be used to reduce the influence of magnetisation direction (Keating and Sailhac 2004; Li 2006; Cooper 2014). However, as can be seen in Fig. 6.1 the total gradient peak is still displaced from the centre of magnetisation by ~12% of source depth. As a further option, the normalised source strength (Beiki *et al.* 2012) provides superior mapping of the horizontal centre of magnetisation that peaks directly over the centre of a dipole magnetisation. Figure 6.2 shows a north–south traverse for sources with horizontal to the north, and vertical-up and vertical-down displacements of 25% of the centre depth. The magnetic field profiles of these sources are inverted with free magnetisation direction in attempted compensation for the enforced spatial offsets (note that for this and all other model profiles shown in this paper inversions are best-fitted not just to data on the displayed individual profile but to the complete anomaly). The enforced horizontal source displacements shown in

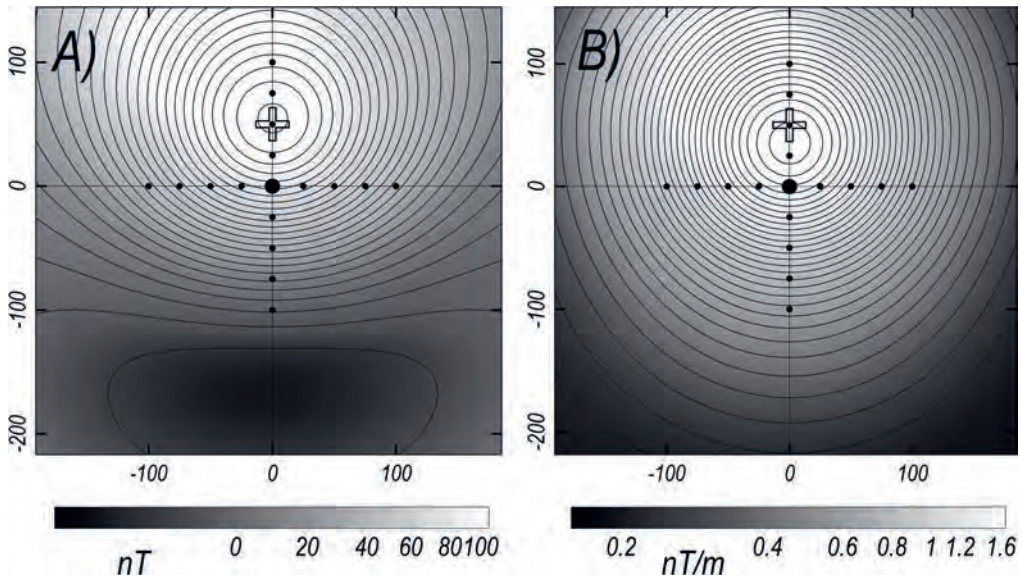

Fig. 6.1. Test dipole centre locations plotted over A) TMI, and B) the total gradient of TMI, for a magnetic dipole (magnetisation 0°, −60°) with centre (0,0, depth 200 m) in a geomagnetic field of (0°, −60°). The cross marks the location of the horizontal-offset dipole in Fig. 6.2.

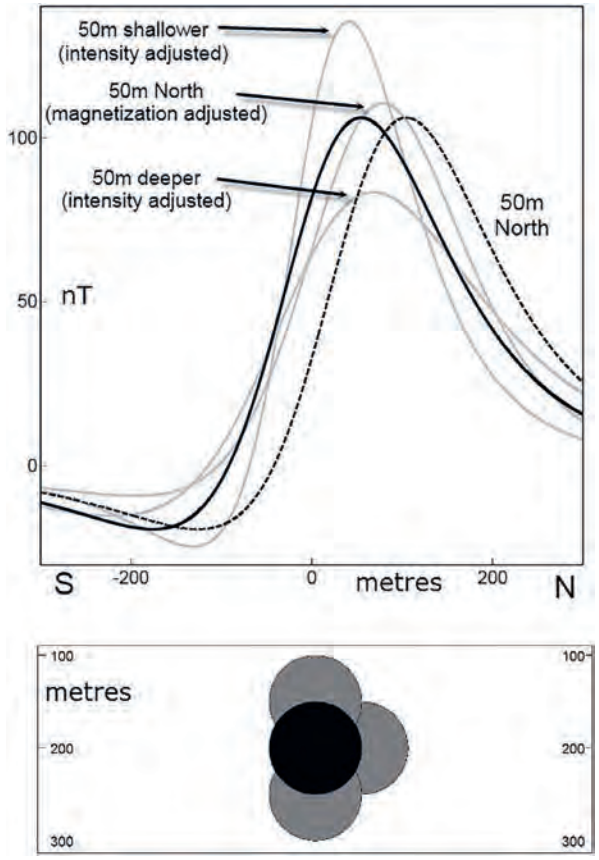

Fig. 6.2. South to north section and TMI profiles through dipole anomalies: reference (black solid line), 50 m north offset (dashed line) and post-inversion compensation by magnetisation changes (grey lines).

Fig. 6.2 are partially compensated by adjustment of magnetisation direction but not to the extent that the magnetic field of the correctly positioned and spatially offset sources are closely matched. The change in magnetisation direction to best compensate for the offset returns the location of the peak of the anomaly by only about one-half of its initial displacement and there is substantial residual data misfit. Vertical offsets of the dipole produce changes predominantly in amplitude and sharpness of the anomaly. The influence of a vertical displacement is partially compensated by adjustment of the intensity but not direction of magnetisation.

Plots of post-inversion data misfit against spatial offset of the source are shown for a range of horizontal and vertical displacements in Fig. 6.3. In most cases there is an almost linear increase of data misfit with the offset distance. Inversion of magnetisation intensity reduces data misfit by ~50%. At a conservative detection level of a normalised data misfit of 0.1, horizontal source offsets are less than 4% of source depth. This reveals that change of magnetisation direction can only compensate effectively for small errors in horizontal location of a magnetisation. Figure 6.4 shows that the magnetisation directions from inversion of horizontally offset sources are systematically rotated according to the direction of spatial offset. Horizontal offsets of 50% of source depth to the north, north-west or north-east cause rotation of the estimated magnetisation by over

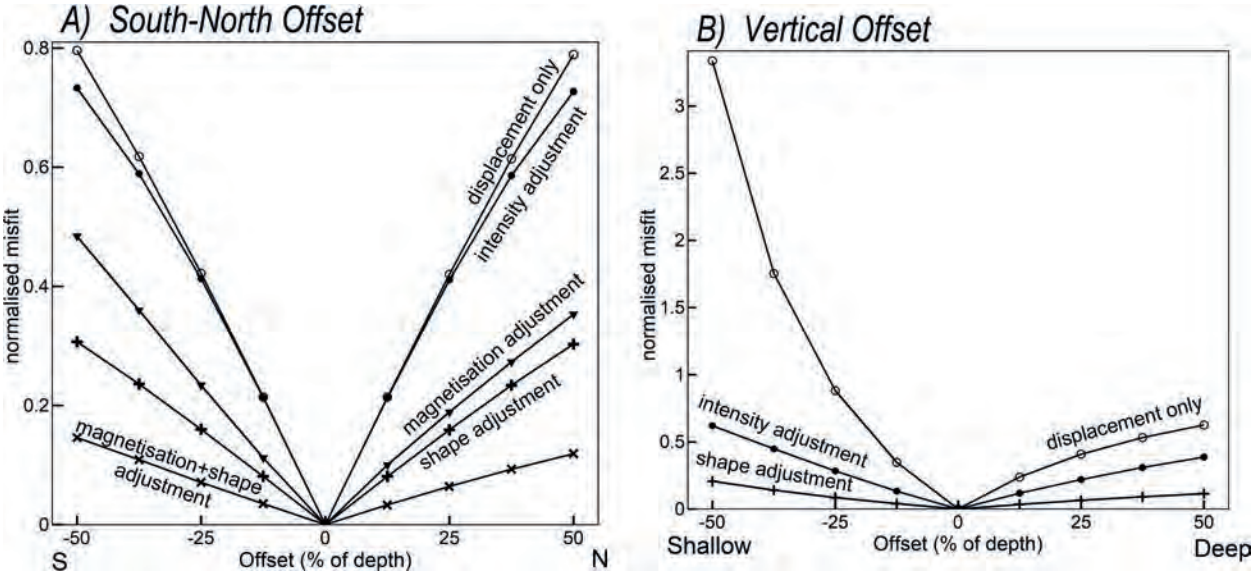

Fig. 6.3. Normalised misfit between the TMI fields of a reference dipole and north–south horizontal and vertical offset dipoles following inversions of intensity of magnetisation and total magnetisation.

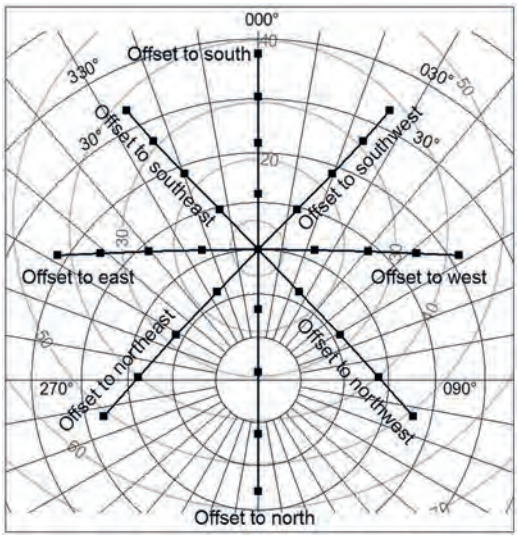

Fig. 6.4. Magnetisation directions recovered from inversion of TMI fields of horizontally displaced dipoles, with contours of angular separation from the reference (0°, −60°) magnetisation direction.

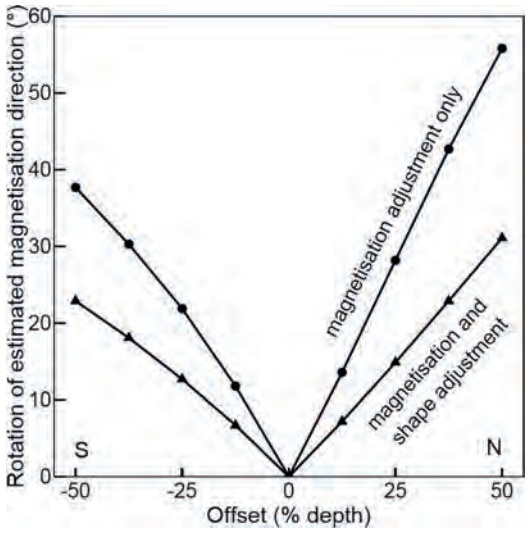

Fig. 6.5. Angular rotation of estimated magnetisation direction from inversions of magnetisation only, and magnetisation and shape for south-north horizontal dipole displacements.

50° but with substantial residual data misfits that clearly reveal inadequacy in representation of the magnetisation. Figure 6.5 plots the angle of rotation of magnetisation direction to best compensate for a horizontal source displacement along a south to north traverse. The rotation is of the order of one degree for a horizontal offset of 1% of source depth. Together with the maximum expected error in horizontal position of 4% of depth, this suggests a corresponding maximum unrecognised error in magnetisation direction of ~4° associated with source displacement only. Change of magnetisation direction alone is not an effective compensation for mis-location of a source, and conversely source mis-location by itself should not cause substantial undetected error in estimation of magnetisation direction.

6.3 INFLUENCE OF SOURCE SHAPE ALONE

For an unknown magnetisation we need to consider to what extent its shape distribution might influence estimation of magnetisation direction. I classify shape as an elongation or shortening of the body along horizontal or vertical axes. I classify elongation or shortening along plunging axes separately as plunge. Figure 6.6 shows tabular bodies and ellipsoids with horizontal and vertical axes of 3:1, longest axis to depth-to-centre ratios of 1.5:1, and longest axis to depth-to-top of ≥ 2:1. The axial ratios of these ellipsoids and tabular bodies are identical but the tabular body is a more substantial departure from a dipole because it retains constant thickness along the extent of each axis whereas ellipsoids are centrally weighted and taper along their axes.

Figure 6.7 shows TMI maps for a dipole and the tabular bodies shown in Fig. 6.6 with magnetisation parallel to the geomagnetic field vector of (0°, −60°). The tabular body with vertical elongation (Fig. 6.7D) produces an anomaly with similar appearance to that of the dipole. The TMI map images of the bodies with the 3:1 ratio of horizontal axes (Figs 6.7B and 6.7C) clearly indicate the orientation of those bodies. Figure 6.8 shows a central section through a dipole and co-centred bodies of identical magnetic moment with both vertical and horizontal north–south elongation. The vertically

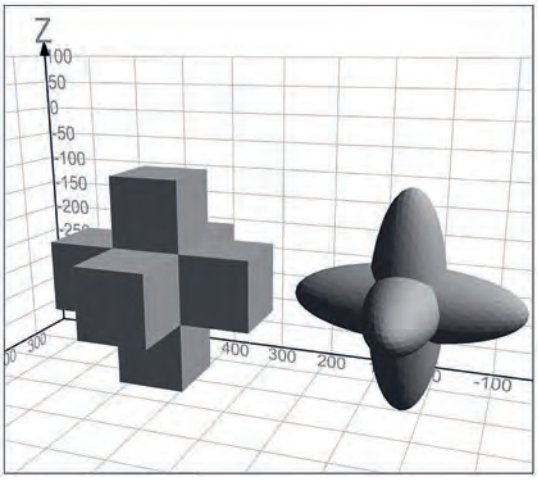

Fig. 6.6. Perspective view of 300:100:100 m axis ellipsoids and tabular bodies.

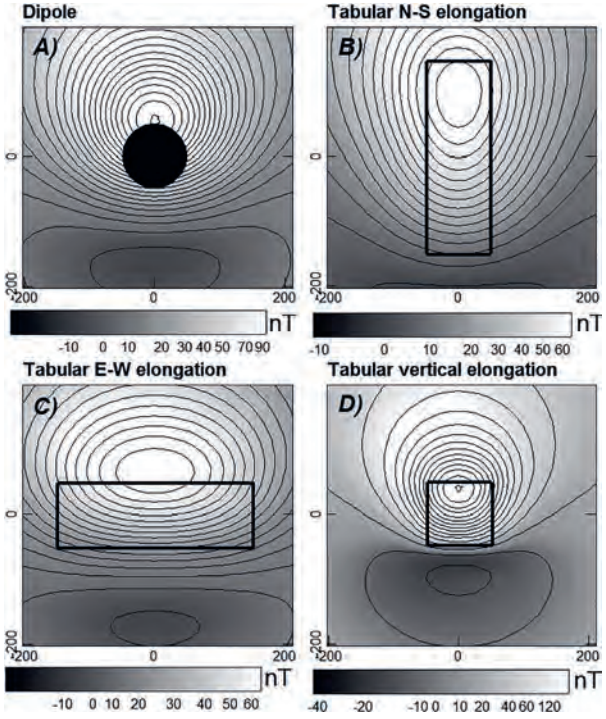

Fig. 6.7. TMI maps (in a geomagnetic field 0°, −60°) for A) dipole, and 3:1:1 elongated tabular bodies: B) horizontal north–south, C) horizontal east–west, and D) vertical.

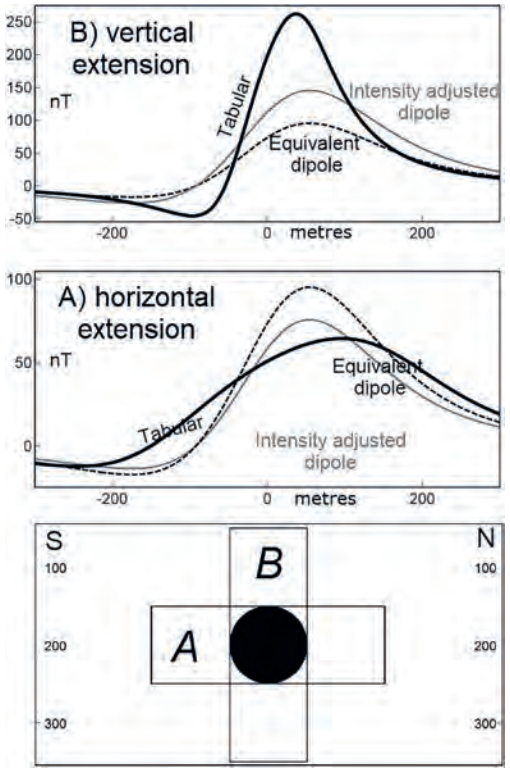

Fig. 6.8. South to north section and TMI profiles for co-centred dipole and pre- and post-inversion elongate tabular bodies and co-centred dipole. TMI profiles of the tabular bodies (inversions of the full anomalies not just the data in this section).

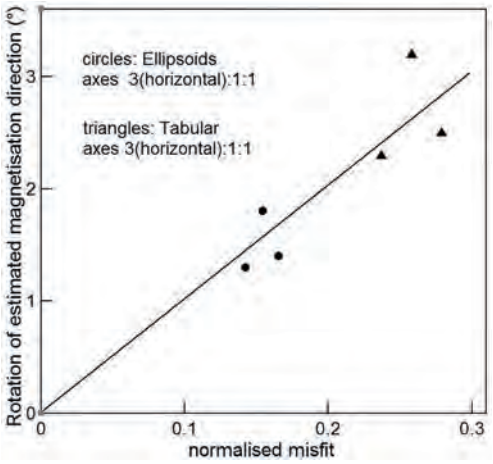

Fig. 6.9. Rotation of estimated magnetisation direction and post-inversion normalised misfit of computed TMI for co-centred N-S, E-W and SW-NE elongated ellipsoids and tabular bodies.

elongated magnetisation produces a field variation with substantially higher amplitude than the dipole due to its extension to shallower depth, but this difference is partially compensated by adjusting the intensity of magnetisation without change of magnetisation direction. For the horizontal elongation the best match to a co-centred dipole is also primarily by adjustment of the intensity of magnetisation, but in this case a slight additional improvement of fit is achieved with minor rotation of the estimated magnetisation direction of between 1.3° and 1.8° for the ellipsoids and between 2.3° and 3.2° for the tabular bodies. As shown in Fig. 6.9, the associated data misfits all have normalised values greater than 0.1 that should be recognised as significant. Extrapolation of the results in Fig. 6.9 suggests that normalised data misfit values of < 0.1 are all associated with rotations of magnetisation direction < 1°. Therefore, within the definition bounds of a compact source, uncertainty of the shape is not by itself a concern in estimating magnetisation direction.

6.4 INFLUENCE OF SOURCE PLUNGE ALONE

3D analysis of compact magnetisation does not suffer from the same exact trade-off between magnetisation direction and plunge as two-dimensional analysis but there is nevertheless quite effective cross-compensation between these parameters. Figure 6.10 shows ellipsoids and tabular bodies with axis ratios 2.5:1:1, long axis to depth-to-centre ratios of 1.25:1, and long axis to shallowest depth ratios of 3.2:1 (outside the conservative definition of a compact source). These bodies plunge 45° to

north, south, east and west. The TMI maps for the tabular bodies plotted in Fig. 6.11 show clear departures from a dipole anomaly pattern, but only subtle characteristics by which that departure can be recognised as due to plunge rather than horizontal shape. To investigate rotation of estimated magnetisation direction due to plunge, I best-matched anomalies of the plunging ellipsoids and tabular bodies using dipole, vertical ellipsoid and vertical tabular sources. Figure 6.12 shows the central profile through a

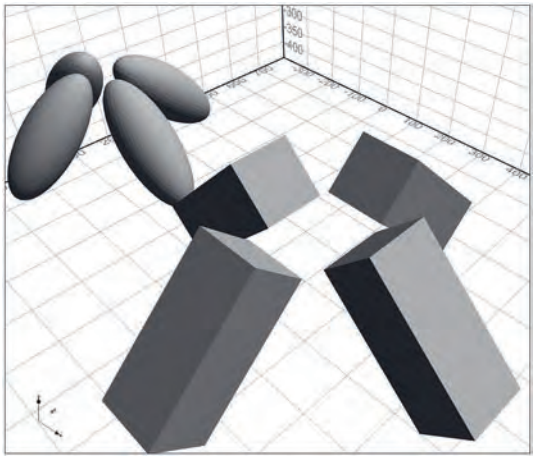

Fig. 6.10. Perspective view of 250:100:100 m axis ellipsoids and tabular bodies with 45° plunge to North, South, East and West.

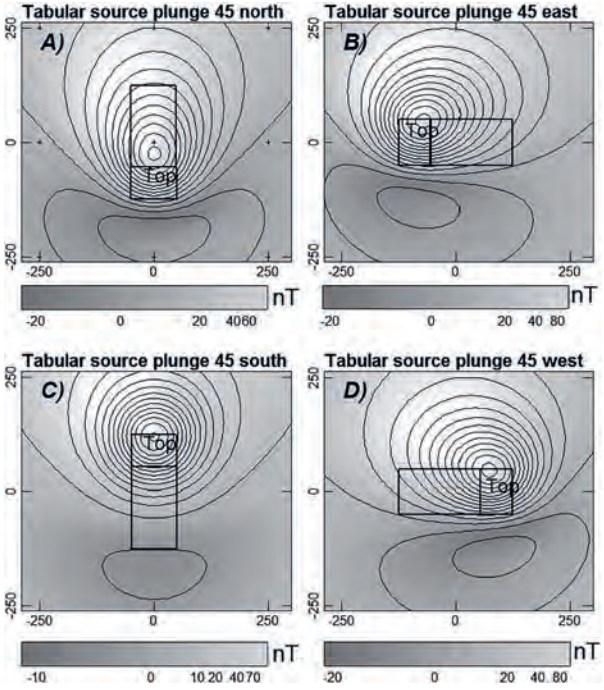

Fig. 6.11. TMI maps for 45° plunging tabular bodies with magnetisation directions (0°, −60°) in a geomagnetic field (0°, −60°). Plunges: A) North, B) East, C) South, D) West.

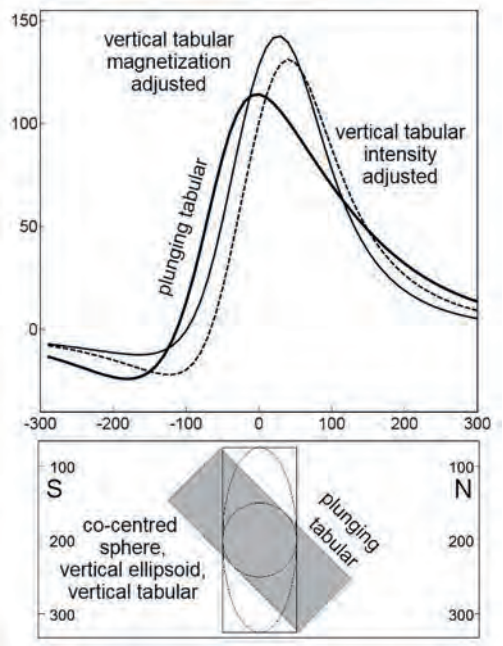

Fig. 6.12. South to north section through a 45° north plunging body and co-centred dipole, vertical ellipsoid and vertical tabular body. TMI profiles are shown for the plunging body, and for the intensity inverted and total-magnetisation inverted vertical tabular bodies.

tabular body plunging to the north and the best-fit co-centred dipole, vertical ellipsoid and vertical tabular bodies. The rotation of magnetisation in attempted compensation for the incorrect plunge of the body is 15° but the normalised data misfit is 0.23 and the models are clearly unacceptable.

Figure 6.13 is a cross-plot of the pre- and post-inversion normalised misfits between computed fields of plunging ellipsoid and tabular bodies with fields of co-centred dipole and vertical ellipsoid and tabular bodies. Figure 6.15A shows results from inversion of intensity of magnetisation alone, and Fig. 6.15B shows results from inversion of both intensity and direction of magnetisation. For both the ellipsoid and tabular bodies, inversion of the intensity of magnetisation reduces the initial misfit by ~20% and inversion of intensity and direction of magnetisation reduces it by a further 20%. The error in estimated magnetisation direction increases with data misfit as shown in Fig. 6.14 with a trend that reveals that normalised misfits of < 0.1 are restricted to errors in magnetisation direction of < 7°.

Figure 6.15A plots the apparent magnetisation direction for dipole and vertical tabular and ellipsoid bodies best-fitted to co-centred ellipsoid or tabular bodies with 45° plunge and magnetisation direction of

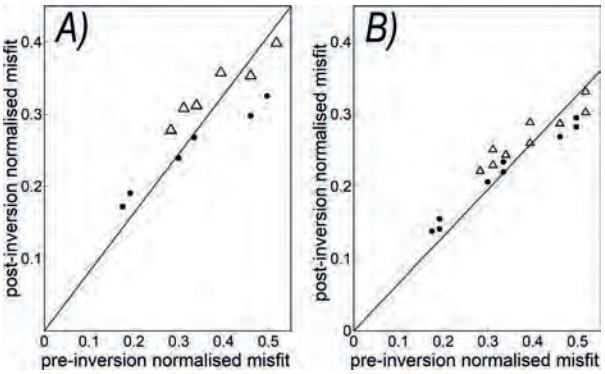

Fig. 6.13. Normalised data misfit between TMI fields computed from 45° plunging ellipsoid and tabular bodies and best-fit dipole and vertical bodies: A) after inversion of intensity of magnetisation, B) after inversion of total magnetisation.

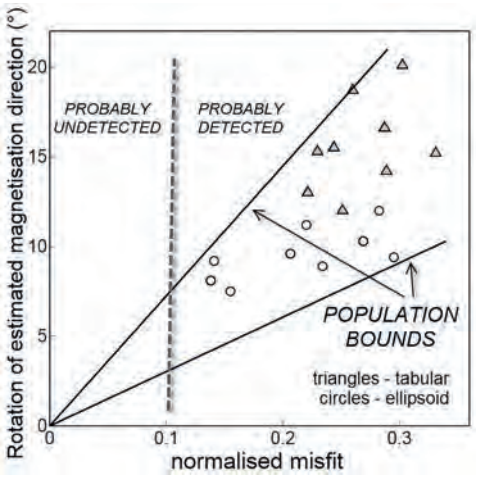

Fig. 6.14. Rotation of magnetisation against normalised misfit after inversion of total magnetisation of dipoles and vertical bodies to match the fields of 45° plunging ellipsoid and tabular bodies. The extrapolated maximum rotation of magnetisation at a normalised misfit of 0.1 is ~7°.

declination 0°, inclination −60° (the triangular symbol in Figs 6.15A and 6.15B). Rotation of apparent magnetisation direction away from the true direction to compensate for enforcement of erroneous plunge is of variable magnitude for different combinations of input and inversion model body geometries, but is in all cases anti-parallel to the direction of plunge. The relationships shown in Fig. 6.15B are discussed in a later section.

Figure 6.16 shows the relationship between error in plunge and corresponding error in estimated magnetisation direction for a range of plunge angles from vertical to horizontal in a north-east direction. Rotation of magnetisation direction is a maximum for a 45° plunge as already investigated, and reduces almost symmetrically to zero for near-vertical and near-horizontal plunge. The results of this study into the ability of error in estimated plunge to compensate for error in estimated magnetisation direction indicate that error in plunge is by itself unlikely to cause unrecognised error in magnetisation direction any greater than 7°, with a maximum for a plunge angle of 45°. Magnitudes of error in estimated magnetisation direction accommodated by variation of other single source parameters as investigated above are listed in Table 6.1.

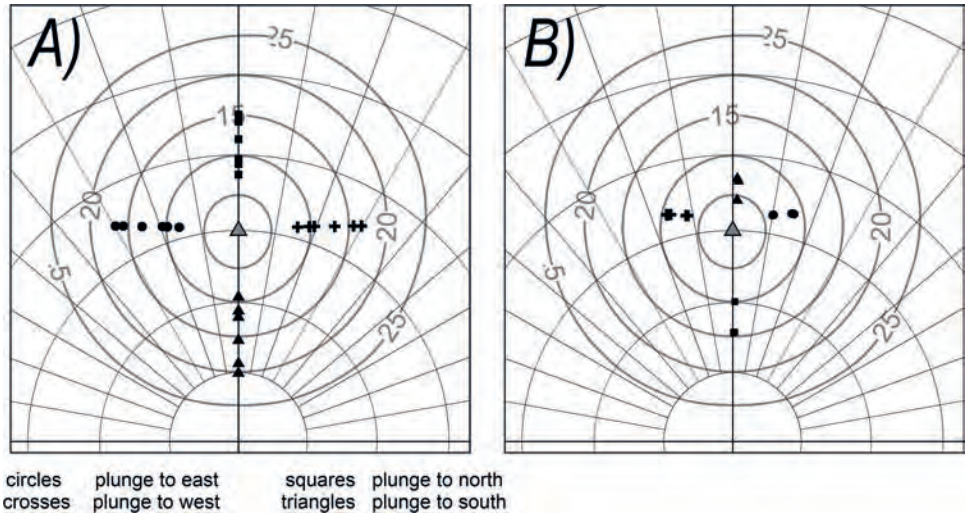

Fig. 6.15. Magnetisation direction plots of dipoles and vertical ellipsoid and tabular bodies best-fitted to 45° plunging ellipsoids and tabular bodies of true magnetisation direction 0°, −60° (marked by the triangle) with contours of angular rotation from that direction for inversion of A) magnetisation only, B) position and magnetisation.

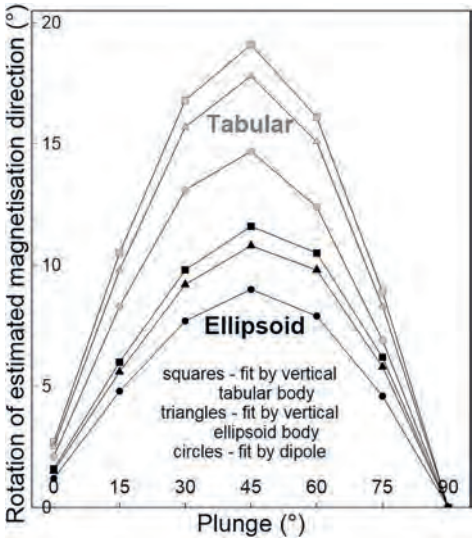

Fig. 6.16. Rotation of magnetisation direction of dipole, vertical ellipsoid and vertical tabular body inversions to match the fields of ellipsoids (black symbols) and tabular bodies (grey symbols) plunging to the north-east.

Table 6.1. Individual contributions of other single parameters to estimation of magnetisation direction for a compact source generating a well defined anomaly.

Model parameter	Uncertainty contribution
Horizontal position	4°
Vertical position	0°
Shape – horizontal extent	1°
Shape – vertical extent	0°
Shape – plunge	7°

6.5 COMBINED INFLUENCE OF SOURCE POSITION AND SHAPE

Inversion of magnetic field data over buried sources requires simultaneous solution of all source parameters rather than isolated solution of individual parameters as previously considered and summarised in Table 6.1. Figures 6.17 and 6.18 show inversion for a spatially offset dipole (as illustrated in Fig. 6.1) for the case that shape is also unknown. For this I replace the spherical model of a dipole with an ellipsoid model that can then be reshaped by the inversion. Results for horizontal offsets are shown in Fig. 6.17. The TMI misfit introduced by the horizontal offset of the magnetisation is substantially reduced by inversion of shape introducing a resulting plunge such that the magnetisation is shallower in the direction from which the body has been offset. Inversion of magnetisation intensity and direction is less effective in reducing data misfit than is inversion of shape. A slight further

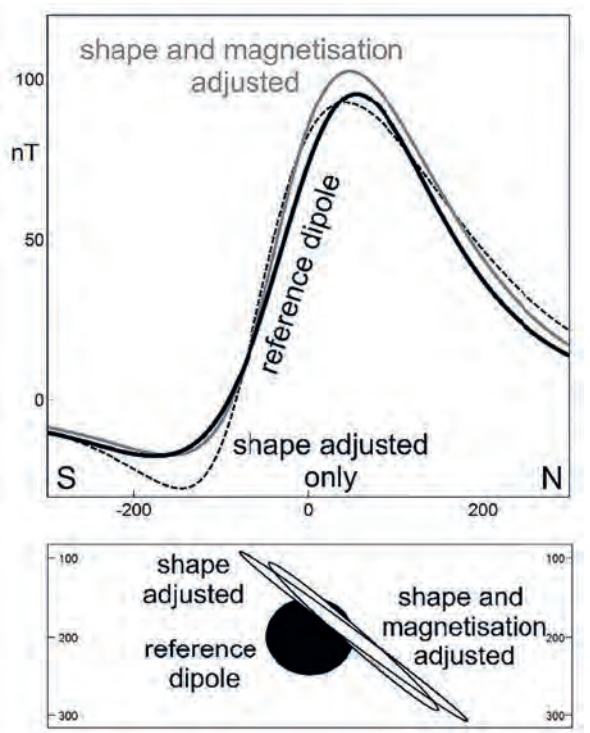

Fig. 6.17. South to north section and TMI profiles for a reference dipole and horizontally (northward) displaced ellipsoids of inversion-adjusted shape and magnetisation.

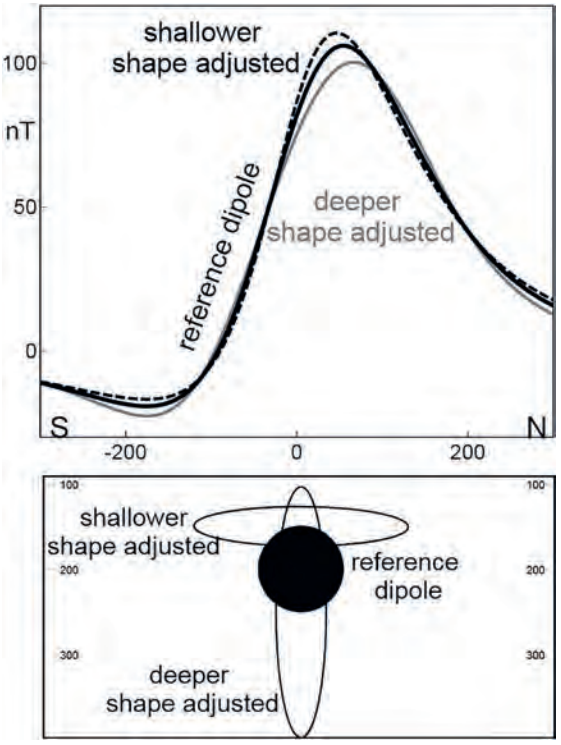

Fig. 6.18. South to north section and TMI profiles for a reference dipole and vertically displaced ellipsoids of inversion-adjusted shape.

reduction of data misfit is, however, achieved by inverting simultaneously for both shape and magnetisation direction. Figure 6.18 shows that in compensation for vertical displacement, inversion of shape is also more effective than inversion of magnetisation. For a vertical displacement, inversion of magnetisation introduces change exclusively in its intensity with no change in its direction.

Figures 6.19 and 6.20 plot the magnitude of post-inversion misfit as a function of offset distance for shape-and-magnetisation inversions. For vertical source offsets (Fig. 6.19) the results clearly show the more effective change of shape rather than magnetisation in compensation for vertical offset. Change of magnetisation direction does not reduce misfit and is not plotted. For horizontal source offsets (Fig. 6.20) change of shape is also more

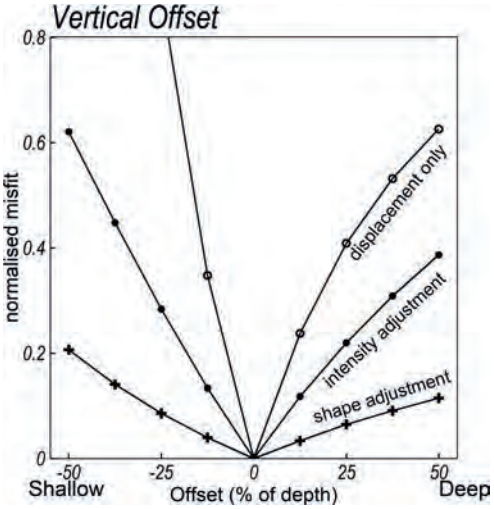

Fig. 6.19. Normalised misfit of inversions to compensate for vertical source offset.

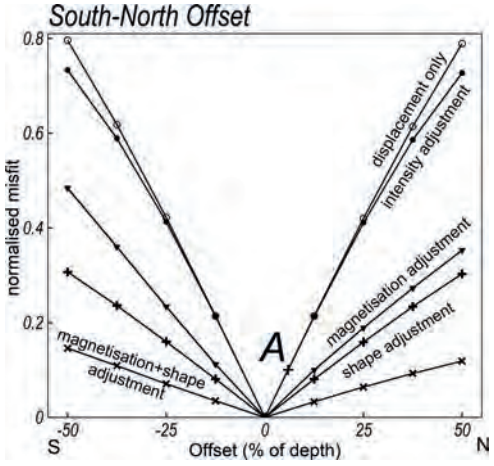

Fig. 6.20. Normalised misfit for inversions to compensate for horizontal source offset.

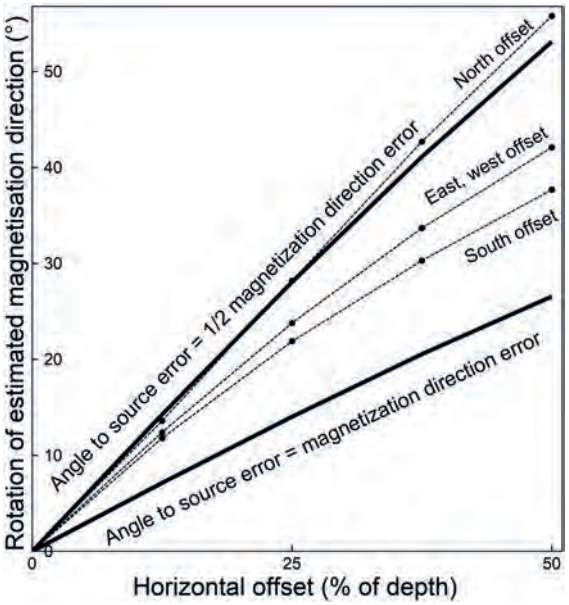

Fig. 6.21. Rotation of magnetisation direction in compensation for horizontal offset of a magnetisation without shape adjustment.

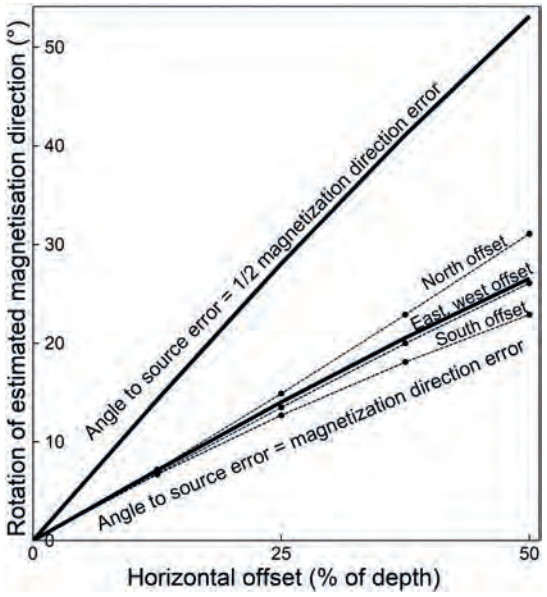

Fig. 6.22. Rotation of magnetisation direction for horizontally offset magnetisations including shape adjustment.

effective than change of magnetisation in compensating for horizontal displacement of magnetisation. In the examples studied, combined shape and magnetisation changes, halve the residual data misfit due to change of shape or change of magnetisation individually.

The magnitude of rotation of magnetisation direction to compensate for horizontal displacement as plotted in Fig. 6.21 varies with direction of horizontal displacement. For the magnetisation direction investigated of

inclination −60°, inclination 0° a northerly displacement is compensated by rotation of magnetisation direction at a rate corresponding to approximately twice the angle to the centre of spatially displaced magnetisation. From the northly displacement-only curve in Fig. 6.20 a normalised misfit of 0.1 corresponds to a horizontal offsets of ~7% (point 'A') and therefore (from Fig. 6.21) a rotation of magnetisation of ~8°. The same data misfits for displacements to east, west and south correspond to smaller magnetisation rotations of 5° to 6°.

Rotation of magnetisation to compensate for horizontal displacement while also allowing simultaneous adjustment of shape is plotted in Fig. 6.22. The additional freedom in this inversion reduces data misfit by 50%, making displacements more difficult to detect. However, the corresponding rotations of magnetisation are also reduced by a factor of 2 and therefore sensitivity to magnetisation direction does not change significantly. The results in Fig. 6.22 fall close to the line of equivalence between angle of offset to source and angle of rotation of estimated magnetisation, suggesting that it is a reasonable approximation that (correcting if necessary for flying height of aeromagnetic data) angular uncertainty in targeting the centre of a compact source giving rise to a well-defined magnetic anomaly is similar to the angular uncertainty of its magnetisation direction. The angles themselves depend on the quality and sufficiency of the data which defines the anomaly, and in favourable circumstances may be of the order of 5° to 8°.

6.6 COMBINED INFLUENCE OF SOURCE POSITION, SHAPE AND PLUNGE

The previous section considers combined variation of magnetisation, position, and shape but from the earlier investigations the most influential individual spatial parameter is plunge. Detection of error in magnetisation direction associated with simultaneous inversion of source shape, plunge and magnetisation is addressed in Fig. 6.23. Inverting for source shape and plunge together with magnetisation intensity and direction for displaced sources (the closed symbols in Fig. 6.23) reduces both the data misfit and the rotation of estimated magnetisation direction from a magnetisation-only inversion (the open symbols). Unfortunately, because inversion of both parameters together reduces the data misfit at a greater rate than it reduces the compensating change in magnetisation direction, there is a resulting net reduction in sensitivity to magnetisation direction. Most of the

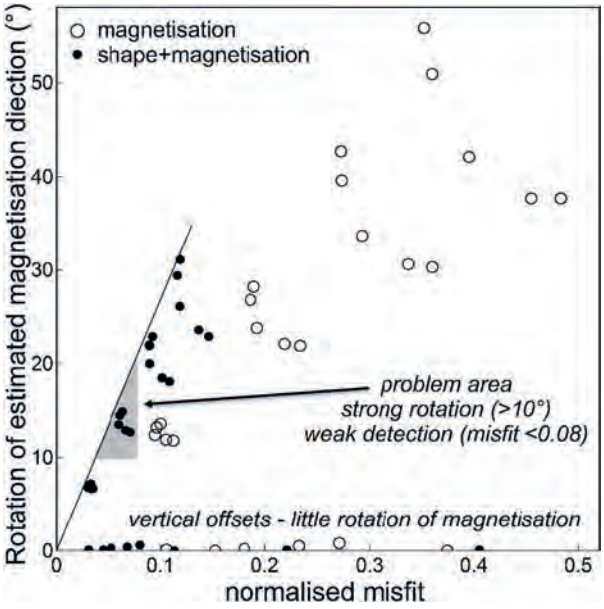

Fig. 6.23. Rotation of estimated magnetisation direction against data misfit for magnetisation-only inversions (open circles), and combined magnetisation and spatial inversions (closed circles). Note that there is almost no rotation of estimated magnetisation direction for vertical source displacements.

combined inversion results have either small rotations in estimated magnetisation direction or high data misfits, but there are a few results with rotations > 10° and misfits < 0.08 (the shaded region in Fig. 6.23) that can pose problems in magnetic field interpretation. These solutions are for horizontal offsets of approximately one-quarter of the depth to their centres, for which (as shown in Fig. 6.17) the optimum source solutions develop a false plunge.

6.7 SUMMARY OF THE SENSITIVITY STUDY

Table 6.2 reviews what I believe to be the key features of this complex analysis. Points are mostly listed in the sequence in which they are addressed in the text. I have tried to make this a comprehensive investigation of the magnetic field expressions of inter-relationships between different features of a magnetisation and its spatial distribution, but it samples only a small part of the full multi-parameter model space. Specific details of the relationships vary with geomagnetic inclination and direction of magnetisation. However, the general conclusions regarding influence of source position, shape and plunge are applicable across all geomagnetic inclinations and for most source magnetisation directions.

Table 6.2. Summarised results of the parametric studies.

1	Estimation of magnetisation direction is fundamentally a three-dimensional problem.
2	Vertical displacement of a dipole source does not in itself introduce significant undetectable error in estimated magnetisation direction.
3	Horizontal displacement introduces rotation of estimated magnetisation direction at the approximate rate of 1° for horizontal offsets of 1% of depth.
4	For a well-defined anomaly due to a compact magnetisation, errors due to incorrect positioning and associated incorrect magnetisation direction should become apparent at horizontal offsets of ~4% of depth and rotations of 4° respectively.
5	For a compact source, the effect of erroneous vertical elongation does not rotate the estimated magnetisation direction. For erroneous horizontal elongation there is only slight shape effect on estimated magnetisation with rotations of < 3° at normalised misfits < 0.1.
6	Erroneous plunge of a body causes greater uncertainty in estimated magnetisation direction than erroneous horizontal elongation, but for compact sources uncertainty in estimated magnetisation direction due to plunge alone is in most cases < 7° at normalised misfits < 0.1.
7	The uncertainty in estimated magnetisation direction most relevant to magnetic field interpretation is simultaneous solution of source location, shape, plunge and magnetisation. Most compact source inversions that acceptably fit the synthetic field data have magnetisation direction consistently recoverable to within 10° (many within 5°) but there are some cases of difficult-to-detect errors which may reach 15° at normalised misfits < 0.1.
8	Estimation of magnetisation direction for equidimensional bodies is relatively robust because it is a bulk characteristic rather than a detail (such as depth to top, or shape), and also because it does not have a particularly close pairing with another parameter or parameter set (as for instance do intensity of magnetisation and volume, which are so closely paired that there is generally little sensitivity to either value, only to their product). For bodies of larger depth extent, however, there is an approximate trade-off with dip or plunge that reduces confidence with which magnetisation direction can be recovered.

Note that since detail of source shape is shown to have little effect in estimation of magnetisation direction for compact sources (distal field data), that similar magnetisation direction estimates should be recovered from both parametric and voxel inversions provided they use similar anomaly separations.

The analytic capabilities of this study are provided by parametric inversions that support isolation and study of single components of complex interactive problems. This study suggests that for isolated, well-defined anomalies due to compact sources of homogeneous magnetisation, uncertainty in source position, shape and plunge should not preclude recovering an estimate of that magnetisation direction from inversion of magnetic field data to within a range of 5° to 10°. For less favourable cases, however, errors in magnetisation direction of up to 15° may occur as a result of combined errors in estimation of source location and plunge. Expected errors in estimated magnetisation direction also increase with decreasing data quality or sufficiency and with increasing complexity or diffuseness of the magnetisation and problems of anomaly separation

Relationships established in this study are more cryptic in complex voxel models, but the relationships are valid for a compact magnetisation and its magnetic field regardless of the model description used. If magnetisations are significantly more distributed or with significant internal variation of magnetisation, then the relationships between magnetisation and the magnetic field degrade and inversion results lose significance. Discrete features in the magnetisation that result in discrete features in the magnetic field are essential for inversion to resolve distribution of magnetisation and its direction.

6.8 THE RYLSTONE CASE STUDY

Rylstone lies close to the margin of the Western Coalfield of the Sydney Basin in New South Wales (Fig. 6.24). There are multiple igneous events in the region across a range of ages, including stocks, sills and diatremes of Jurassic to Tertiary age that intrude the Triassic coal measures (Yoo *et al.* 2001) and give rise to prominent magnetic anomalies strongly influenced by both normal and reverse remanent magnetisation. In 1997 the Geological Survey of New South Wales commissioned a 100 m spaced, nominal 50 m terrain clearance heli-mag survey of this rugged area to map the igneous bodies and assess their influence on the coal resource. The survey was flown by Tesla Airborne Geoscience and interpreted by Encom Technology (Encom Technology 1997). Variation in the geometry and remanent magnetisation of the igneous bodies provides a range of anomalies suitable for testing magnetic field analytic and inversion

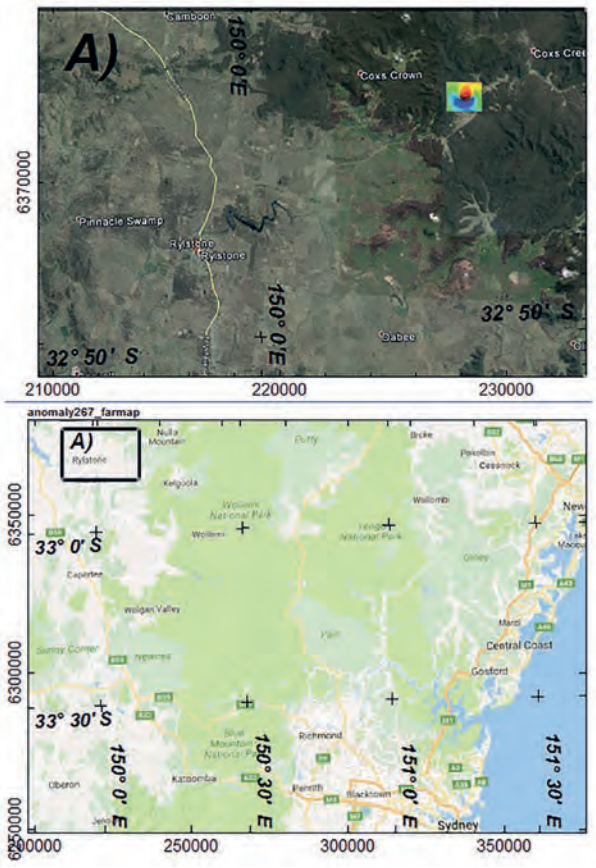

Fig. 6.24. Rylstone Anomaly 267 TMI image over local Google Earth imagery, and B) Regional location of Rylstone area.

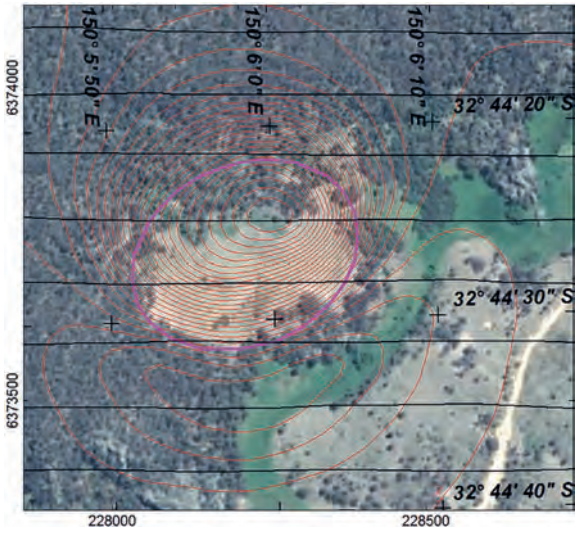

Fig. 6.25. Survey flightlines, TMI contours and elliptic pipe model outline over Google Earth image.

algorithms. In this study I focus on a single anomaly, anomaly 267 in the Australian Remanent Anomalies Database. Figure 6.25 shows the anomaly contours, flightlines and an outline of the modelled source over a

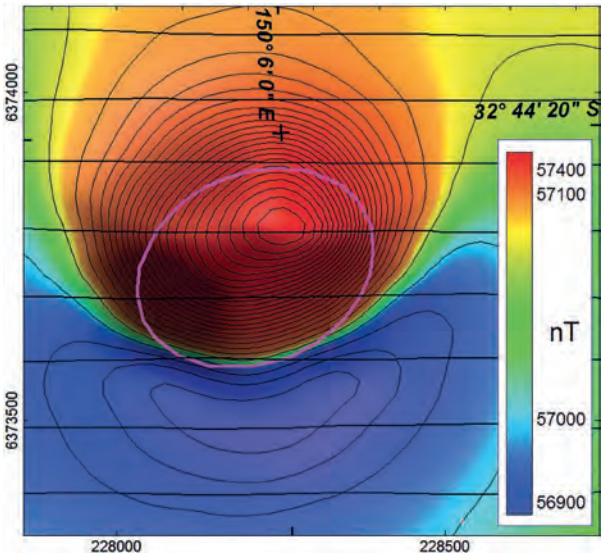

Fig. 6.26. TMI image with flightlines and elliptic pipe model outline.

Google Earth^{TM} aerial image. The anomaly coincides with a clearing that is possibly indicative of volcanic-derived soil but there is no obvious expression of outcrop. The TMI anomaly, that is imaged in Fig. 6.26 has a prominent expression on seven flightlines, a peak to trough range of 1330 nT, and a width of almost 600 m.

6.8.1 Source shape influence in estimation of magnetisation direction

The previous synthetic modelling establishes that estimates of magnetisation direction for a compact source show little sensitivity to the detail of shape. Figure 6.27 shows stacked profiles of TMI computed from the best-fit inversion model of a vertical circular cylinder, together with three of the central flightline sections through the model. All spatial parameters were free to vary in the inversion, as was intensity and direction of magnetisation. The resulting fit to the measured anomaly has a normalised data misfit (standard deviation of the difference between computed and measured data divided by the standard deviation of the measured data) of 0.18. The body has a diameter of 331 m, depth extent of 143 m and minimum depth below measurement sensor of 79 m. The magnetisation direction is declination 347°, inclination −76°. The maximum dimension of the body of 360 m gives a maximum-extent to measurement-proximity ratio of 4.6:1. Also shown in Fig. 6.27 are computed TMI stacked profiles and model sections for the best-fit dipole model. A dipole is a source either so compact that its shape requires no specification, or a

homogeneous sphere of any radius less than the distance from its centre to the ground surface. To constrain the size of the spherical source body (which by itself has no influence on the inversion results) I gave the spherical source the same intensity of magnetisation as the best-fit vertical circular-section cylinder model. The dipole model has a higher inversion misfit statistic of 0.32, and the estimation of magnetisation direction is 10° from that of the vertical circular-section cylinder model. The limitation of this model in matching the data is best illustrated on the highest amplitude flightline 100660 (the topmost model section in Fig. 6.27) which reveals that the dipole model is too centrally weighted to match the data well, producing a sharper anomaly than is measured. Evaluation of the inversion model is subjective, but the improved fit from the vertical circular-section cylinder model suggests that the magnetisation is likely to have a more horizontal distribution (for instance a horizontal top and base) than is represented by a sphere.

To be considered successful, a magnetisation model must explain the complete anomaly. Specific details of the misfit may assist interpretation as illustrated in Fig. 6.27. Figure 6.28 shows model sections and computed fields along the most critical flightline 100660 for best-fit tabular and ellipsoid models. Although those body types are quite different, there is no significant difference between the matches of their computed fields to the measured anomaly and no strong grounds from the inversion results to prefer one model over the other as a representation of the sub-surface magnetisation. Figure 6.29 is a downloaded form from the Australian Remanent Anomalies Database with the details of four alternative source models, each of different geometry. Difficulty in discriminating between these various source model geometries highlights the insensitivity to details of shape in inversion of a compact magnetisation. For an identical anomaly separation a voxel inversion should recover the same magnetisation direction.

The Rylstone area has both sills which can be reasonably represented as horizontal sheets and diatremes that are saucer or funnel-shaped layers of breccia or lava above a thin neck (Yoo *et al*. 2001). The inversion source models are broadly consistent with either of these geological concepts. As shown in Fig. 6.30, each of the source geometries occupies almost the same space. All are near-surface with horizontal extents ~300 m and vertical extents of 50–100 m. The exact geometry of these models should not be interpreted literally but as approximate bounds on the expected distribution of magnetisation. Furthermore, the only constraint on internal inhomogeneity of the magnetisation is that the total magnetisation and its centre location should approximately match those of the homogeneous model. These restrictions arise because the magnetic field measurements are not close enough to the magnetisation to resolve shape details or minor variations of the

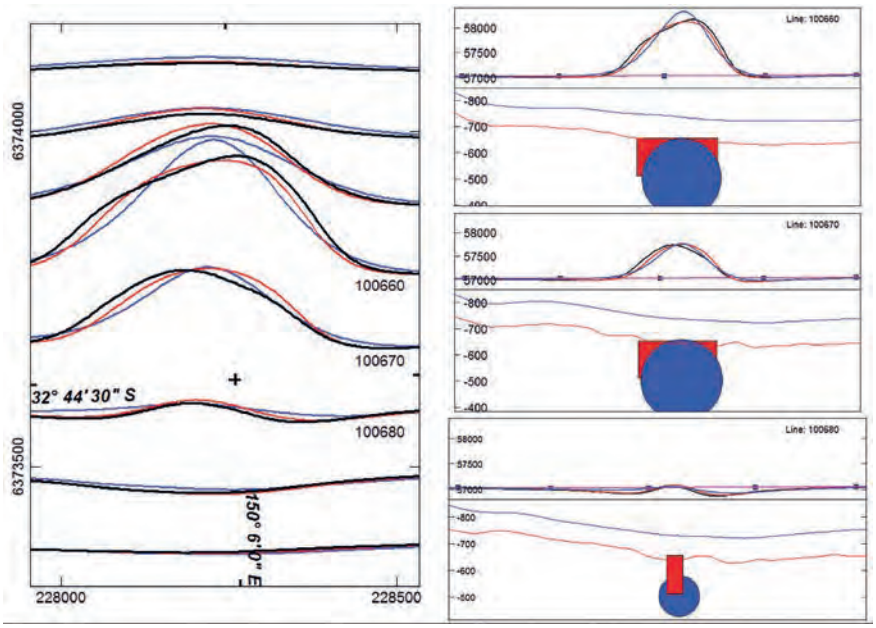

Fig. 6.27. Stacked profile and central model sections for the sphere model (blue) and the vertical circular pipe model (red).

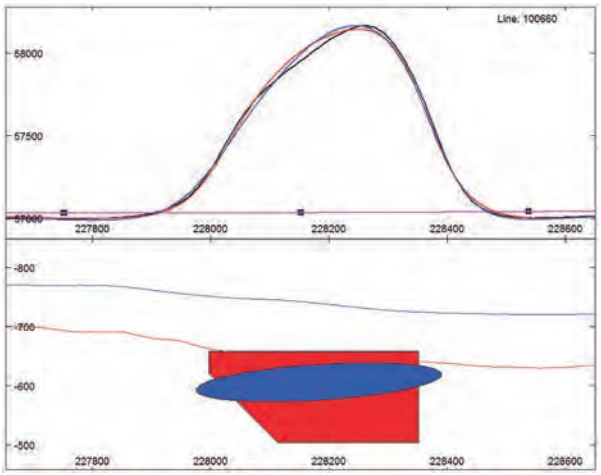

Fig. 6.28. Section along flightline 100660 through plunging tabular (red) and ellipsoid (blue) models.

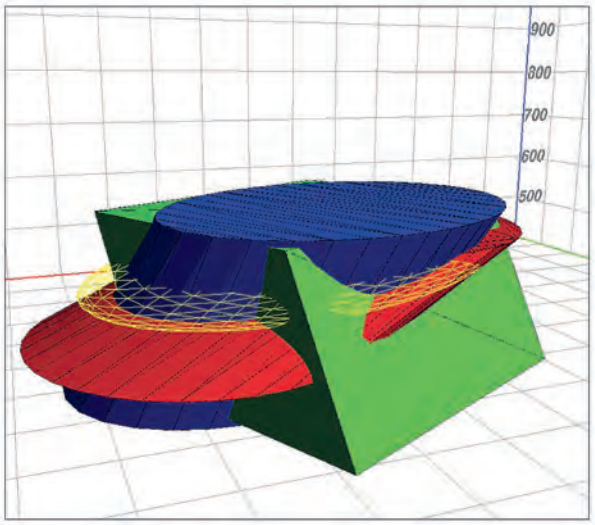

Fig. 6.30. Three-dimensional view of alternative source models.

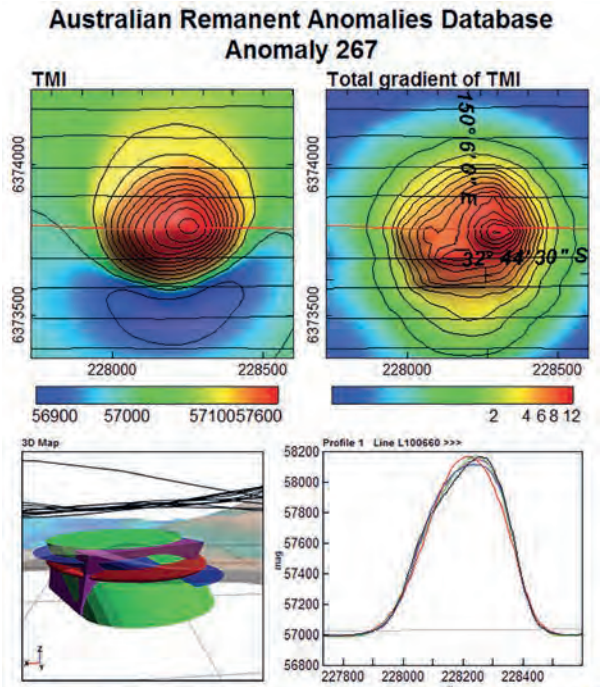

model	Amp/m	Declination	Inclination	volume m^3	moment Amp.m^2
267_280	9.6	34.8	-74.6	6140000	590000000
267_281	4.49	42.9	-79.5	13800000	61800000
267_282	11.3	34.6	-79.3	4840000	54700000
267_283	5.04	357.7	-76.3	12200000	61200000

Fig. 6.29. Anomaly 267 source inversion summary from the Australian Remanent Anomalies Database (model 280 – green, model 281 – blue, model 282 – red, model 283 – purple).

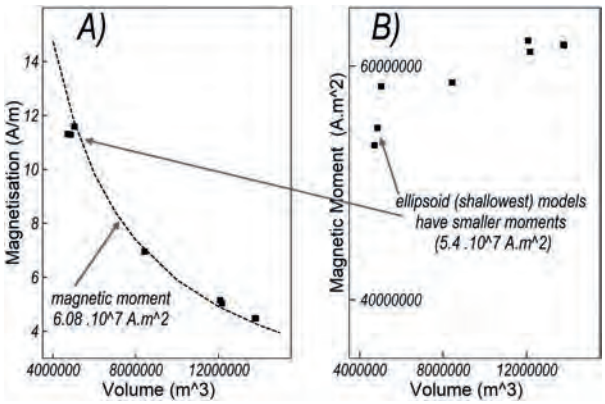

Fig. 6.31. Magnetic moment of best-fit inversion models.

internal distribution of magnetisation. Figure 6.31 shows plots of magnetisation and magnetic moment against volume for these source models. There is a variation of more than a factor of 2.5 in both volume and magnetisation intensity, but the magnetic moments calculated as the products of these two factors vary by less than 10%. The magnetisation directions of the various model bodies are plotted in Fig. 6.32 (the directions are listed in Fig. 6.29). The directions vary by less than 10° and all are less than 7° from the mean direction of declination 26.6° and inclination −78.0°. The 15° separation between the mean direction and the IGRF geomagnetic field for the site suggests that the magnetisation direction has a slight but significant rotation away from the geomagnetic field, most probably due to a remanent magnetisation component. The magnetisation models are not particularly compact with respect to the proximity of the magnetic field measurements. The extent to proximity ratios for the various models are 4.6:1 for the best ellipsoid, 6.0:1 for the best circular-section pipe, 6.4:1 for the best tabular body and 6.8:1 for the best

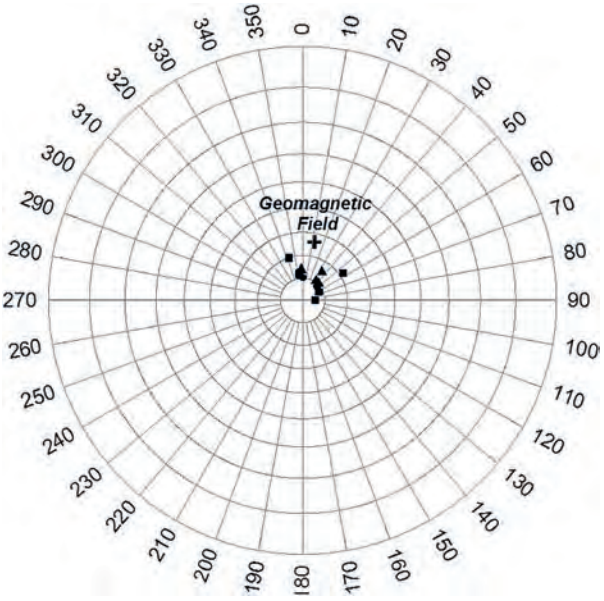

Fig. 6.32. Model (ellipsoid, tabular, circular, elliptic pipes) magnetisation directions from inversion of all lines (triangles), odd-number lines (circles), even-number lines (squares).

elliptic-section pipe. However, even at these values the inversion results are still in good agreement with the conclusion that magnetisation direction can be consistently recovered for compact sources with little influence of body shape (Foss 2017). The corollary of this finding is that for these sources shape is a detail that cannot be reliably recovered from the magnetic field inversions. Unfortunately, because I do not have direct measurement of the Anomaly 267 magnetisation I can only establish consistency and not correctness of the estimated magnetisation direction.

6.8.2 Source position influence in estimation of magnetisation direction

Each of the model inversions presented in the previous section, while primarily testing influence of source shape, was also free to independently position those sources. The consistency of the model results therefore also testifies to the stability in simultaneously estimating source position and magnetisation direction. Figure 6.33 shows the centre points of the various source models together with the outline of the elliptic-section cylinder model over images of measured TMI, computed TMI, total gradient of TMI and the 1:100,000 scale geological map (Yoo 1998). The centres of the source models all plot in an area mapped as undifferentiated Jurassic or Tertiary volcanics which provides a compelling explanation for the anomaly. There is approximately a 50 m spread in the various model centres, which is only 50% of the survey line spacing and less than 15% of the estimated horizontal extent of the source. Surprisingly, the maximum dispersion is along the flightline direction rather than perpendicular to it. There is slight disagreement between the edges of the body as mapped geologically and by the magnetics but this apparent difference may be due to limited (or no) outcrop, inexact location in the pre-GPS geological mapping, or because the geological mapping is intended to note the presence of the volcanics rather than to map their exact extents.

Figure 6.34 shows in more detail the model centres plotted on the total gradient of TMI. There is a broad high in total gradient values at 7 to 8 nT/m, the edge of which coincides approximately with mapping of the extent of magnetisation by the elliptic-section pipe model. The local peak of the total gradient is sharp and irregular, possibly mapping local concentrations of near-surface magnetisation but clearly also strongly influenced by the survey flightline locations.

Figure 6.35 shows the centre points of the various models in 3D space, which reveals that the estimate of vertical centre of magnetisation is also consistently (although not necessarily correctly) recovered. This consistency of position and magnetisation direction supports the previous synthetic data study which established that inversion can reasonably resolve both the centre location and direction of magnetisation of compact sources.

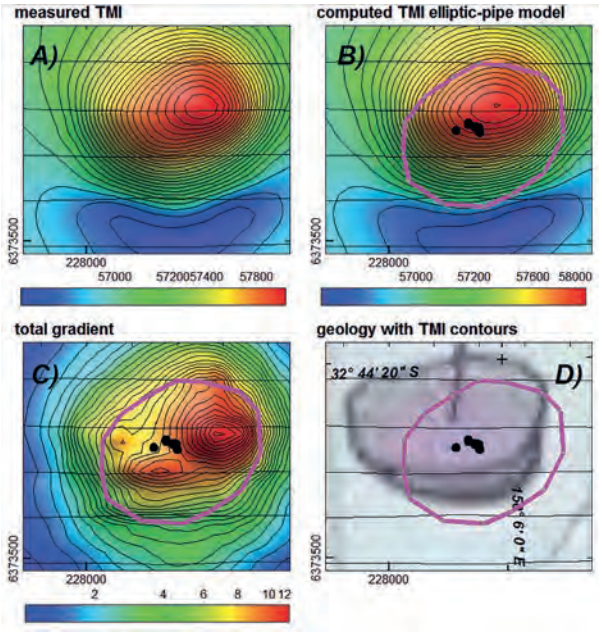

Fig. 6.33. A) measured TMI, B) TMI computed from the elliptic-pipe model, C) total gradient of TMI, ams D) pipe outline over the geological map.

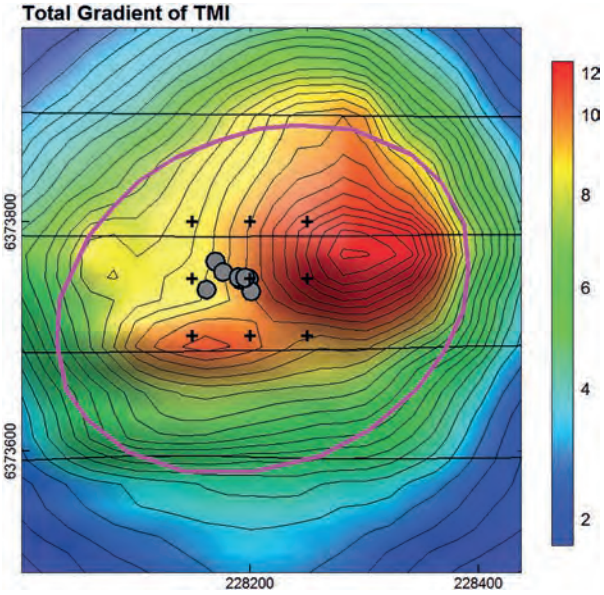

Fig. 6.34. Centres of inverted source models (circular points) and a grid of test body centres (crosses) over a contoured image of total gradient, with the outline of the best elliptic pipe model (magenta).

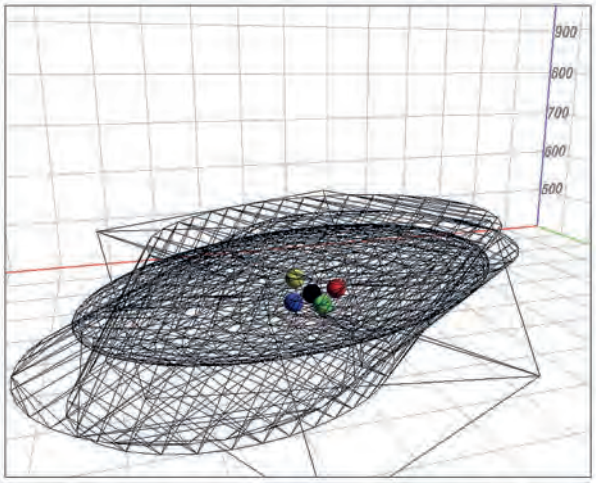

Fig. 6.35. Wireframe perspective of the four source models with their centre points (colour coded as in Fig. 6.30). The black symbol is the mean of the four estimates.

I investigated the influence of source position by imposing displacements on the source models, as in the previous synthetic data study. A three-by-three 50 m grid centred on the best-estimated horizontal centre of magnetisation is plotted in Fig. 6.36. Ellipsoid, circular-section pipe, elliptic-section pipe and tabular models were each centred at the various grid points and inverted to determine the best estimate of magnetisation direction for sources at those locations (the inversions retained the bodies as vertical to prevent migration of the magnetisation centres with plunge). The resulting magnetisation directions from the inversions are plotted in Fig. 6.36. These directions are tightly grouped according to source displacement, with only minor variation between the various body types at any one location. This confirms the synthetic data study finding that for compact sources estimated location is much more strongly linked to magnetisation direction than is shape. The mean elevation difference between the measurements and the centre of magnetisation is 140 m, giving a rotation of estimated magnetisation direction of ~80% of the angle of spatial displacement, consistent with estimates from the synthetic data studies.

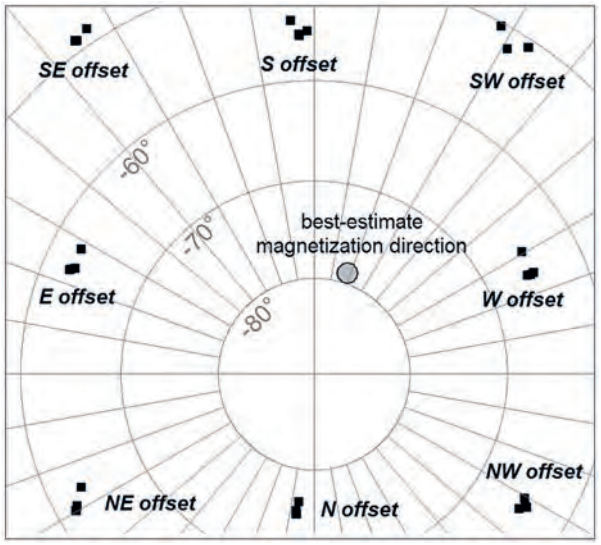

Fig. 6.36. Post-inversion magnetisation direction of bodies with imposed horizontal offsets.

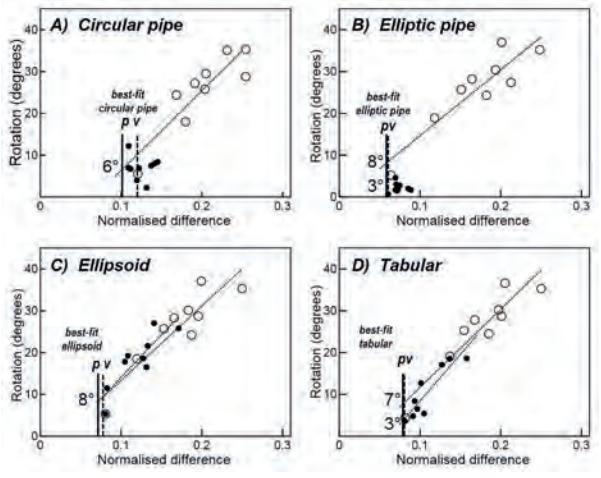

Fig. 6.37. Cross-plots of rotation of magnetisation direction against data misfit for horizontal offset sources: open circles are vertical sources, points are plunging sources.

In Fig. 6.37 rotation angle and data misfit are cross-plotted from the inversions of each of the four body types (both plunging and vertical) offset in the eight directions at 45° intervals. These straight-line relationships are extrapolated to the data misfit values of the best-fit inversions of each body type to estimate the angular error that can be accommodated by that data misfit. The angles range only between 6°and 8° for the different body types and are likely to be overestimates of error in magnetisation direction because much of the data misfit arises from local and uncorrelated irregularities in the data.

6.8.3 Source plunge influence on estimation of magnetisation direction

The previous synthetic data study found that variation in plunge of a body can be traded against variation in its magnetisation direction. Initial inversions of the horizontally offset sources retained their plunge as vertical. I subsequently re-ran the inversions allowing those bodies to plunge. Figure 6.38 shows a map of the axes of the post-inversion circular-section pipe bodies over the shallowest 10 m of their depth extent (this restriction is to reduce confusion where the axes cross each other). The trend of the body axes converge towards the centre of magnetisation, revealing that the inversions utilise their freedom of plunge to compensate for their imposed horizontal offsets. The cluster of the centroids about the best-estimated centre of magnetisation confirm this behaviour (individual centroids overshoot the centre-point to compensate for mis-location of the more influential shallowest sections of the bodies). The same relationships are illustrated in perspective view in Fig. 6.39.

The post-inversion magnetisation directions for each body type are plotted in Fig. 6.40. The various source geometries behave differently to compensate for the enforced horizontal offsets in inversion of magnetisation and plunge. The elliptic-section pipes (Fig. 6.40B) have an average rotation of magnetisation from the best estimated direction of 26° for inversions in which they are not allowed to plunge, but that is reduced substantially to

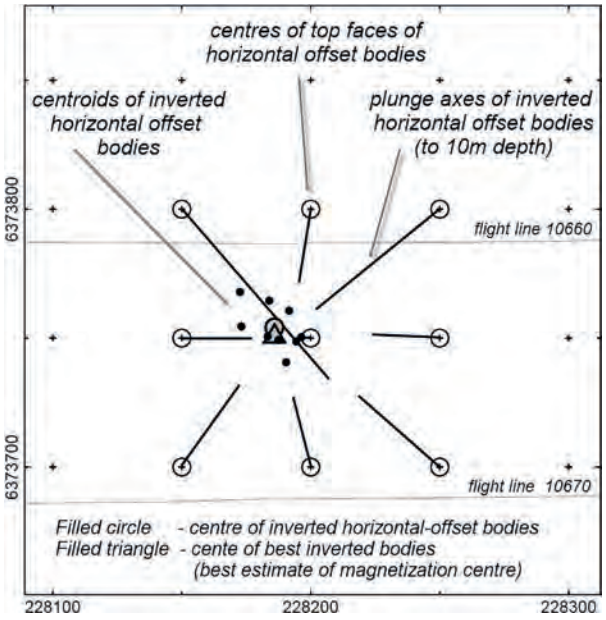

Fig. 6.38. Map of the top face centres (open circles), centroids (points), and plunge axes of the inverted horizontally offset.

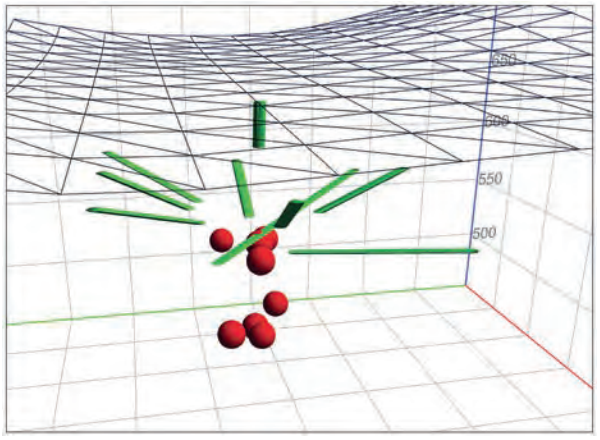

Fig. 6.39. Axes of horizontally offset bodies after inversion allowing plunge (green – shown to only 10 m depth) and centres of magnetisation of those bodies (red).

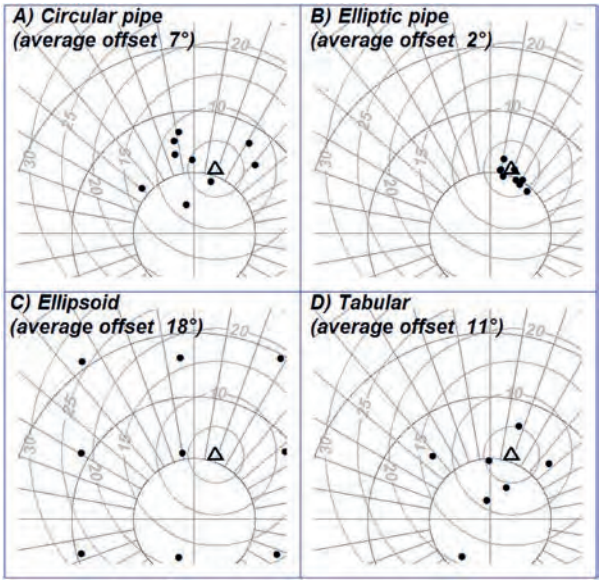

Fig. 6.40. Directions of magnetisation of horizontally displaced sources after inversion of magnetisation direction and plunge.

less than 3° if the bodies are allowed to plunge as well as to change magnetisation direction. The circular-section pipe model inversions (Fig. 6.40A) have fewer degrees of freedom and perform less well, but the average rotation of magnetisation is still reduced from 26° to 8°. Following inversion with free plunge and magnetisation, tabular bodies (Fig. 6.40D) have greater scatter of magnetisation direction and a marginally higher average rotation of 11°. Ellipsoid bodies (Fig. 6.40C) have the largest average rotation of 19° and retain the systematic rotation of magnetisation determined by the direction of imposed horizontal offset for each body. This ineffective compensation of plunge for horizontal offset ellipsoids is because the locked reference point for these bodies is their centre, which does not allow plunge to migrate the centre point (for the other body types the locked reference point is the centre of the top face and plunge migrates the centre of magnetisation). This difference in behaviour disappears for inversions that simultaneously allow position to change as well as plunge.

6.8.4 Sensitivity tests of estimated magnetisation direction

In previous sections I have analysed the influence of source location, shape and plunge on recovery of magnetisation direction to provide a case study test of the synthetic data inversions. An alternative approach to evaluate recovery of magnetisation direction is to perturb magnetisation direction and investigate how effectively other source parameters can compensate for that imposed deflection. Figure 6.41 shows test magnetisation directions offset from the best-estimated direction 10° and 20° towards lower inclination (A), steeper inclination (B), and in orthogonal trends (C and D). The post-inversion data misfits for magnetisations in these offset directions are plotted in Fig. 6.42. The previous synthetic data studies established that post-inversion normalised misfit increases almost linearly in all directions away from the true magnetisation direction (for which the misfit value was zero). For the real data of this case study the minimum normalised data misfit is between 0.06 and 0.11 for different body geometries. The average increase of misfit for each curve over the 20° excursions is 54% of the minimum value, giving curves which still monotonically increase from the minimum but are more of a 'U' rather than 'V' section. With only a single exception, the curves for the different body types share common minima at the 10° sampling interval. These results suggest that by careful inversion, the best magnetisation direction with which the source of Anomaly 267 is represented as a compact homogeneous magnetisation has been resolved to between 5° and 10°. Non-uniqueness does not allow that success of the proposed model necessarily proves that this is a true representation of the subsurface magnetisation. Indeed, most geological bodies are expected to have moderate to extreme internal inhomogeneity, although that may not be detectable in analysis or inversion of even moderately distal magnetic field data.

The lowest data misfit values of three of the models are close to .05. The previous noise-free synthetic data study suggests that at this level of misfit magnetisation direction of compact sources is constrained to better than 5° to 10° (with some rare exceptions). The irreducible data

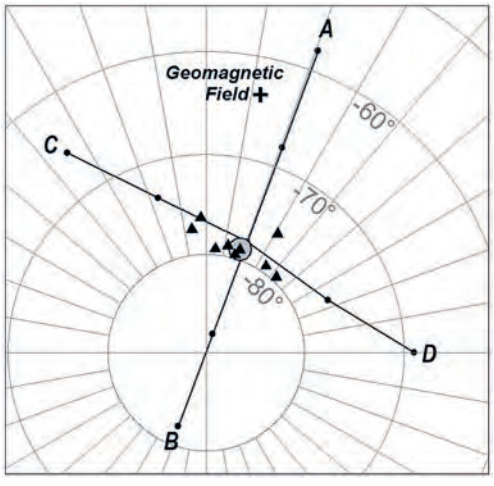

Fig. 6.41. Post-inversion data misfit for rotations of magnetisation: (crosses) circular-section pipe, (squares) tabular body, (triangles) ellipsoid, and (circles) elliptic-section pipe models.

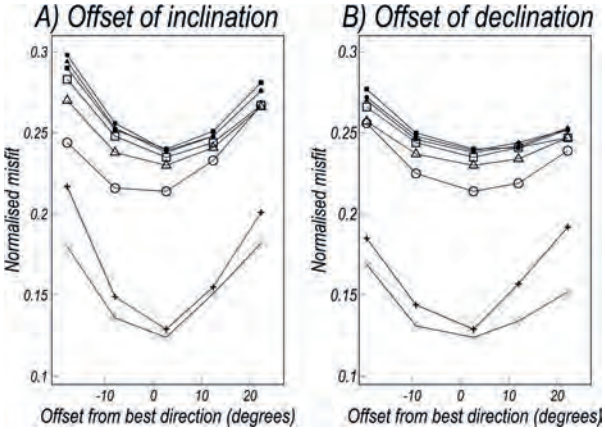

Fig. 6.42. Post-inversion model magnetisations (triangles), mean direction (filled circle) and sensitivity test traverses A-B and C-D with offsets of 10° and 20°.

misfits for the simple homogeneous models in this case study are most probably due to irregularities in the local distribution of magnetisation and/or short-wavelength errors in the magnetic field data acquisition and processing. The maximum extent to data-proximity ratio of between 4.6:1 to 6.8:1 is well outside the bounding value of 2 assumed for a compact source in the synthetic data study, suggesting that magnetisation direction estimates would be even more robust for truly compact sources.

Figure 6.43 shows stacked profiles and a grid image of residual misfit for the best elliptic pipe model. These reveal that post-inversion residual data misfits are local short-wavelength features that are either data artefacts or imperfections of the model at a shallow level. Figure 6.44 shows grid images of difference in the fields computed from the best-fit model and from inversion models with magnetisations 5° steeper and 5° shallower. These images show similar short-wavelength features as in Fig. 6.43, but also low-amplitude, longer wavelength features that extend over at least six flightlines. These features are of opposite polarity for the shallower and steeper magnetisation and are interpreted to be expressions of the misfit caused by enforcement of those inappropriate magnetisation directions. The absence of these features in the residual misfit image of the best model shown in Fig. 6.43 further suggests that the best magnetisation direction has been located to within 5°. Note that these broad, low amplitude features also emphasise the importance of anomaly separation and the sensitivity of the model inversion results to that separation.

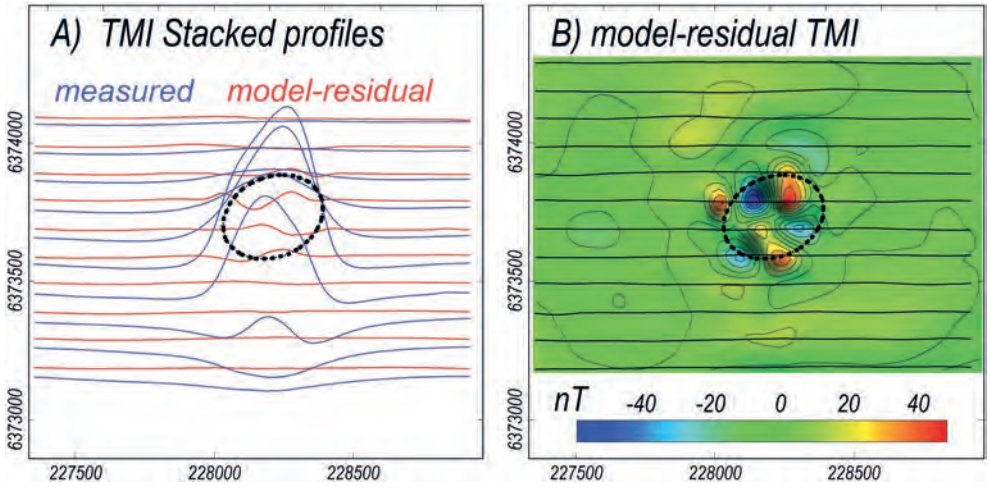

Fig. 6.43. (top) Stacked profiles of measured TMI (blue) and residual misfit (red) for the elliptic pipe model; (bottom) residual misfit from the elliptic pipe model. The dashed line outlines the top of the model.

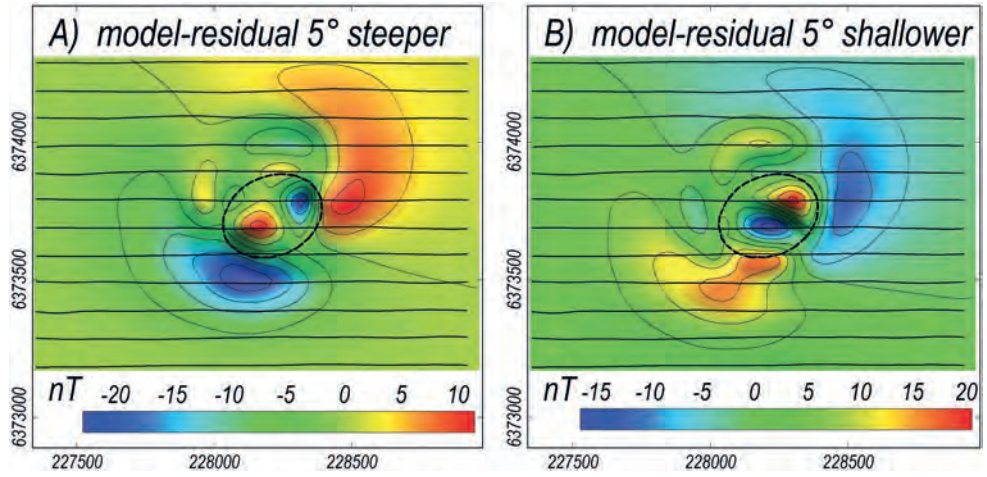

Fig. 6.44. Differences between fields computed from the best elliptic pipe model and best matching elliptic pipes with magnetisation 5° steeper (top) and 5°shallower (bottom).

6.8.5 Data sufficiency tests of estimated magnetisation direction

As discussed above, for this case study it seems feasible with multiple inversions to consistently recover the best-fit homogeneous magnetisation direction to within 5° to 10°. One of the major concerns for small anomalies such as this is that while it may be possible to find the best magnetisation direction to explain the available data, the data itself may be an insufficient or misleading sampling of the complete anomaly. As shown in Fig. 6.26, Anomaly 267 is defined on eight lines, with a significant expression on five of those. North–south lines would have provided a superior sampling of the anomaly because the positive and negative lobes are both sampled on each line. However, with even a coverage of five east–west lines at 100 m line spacing there is enough data redundancy to investigate sufficiency of a 200 m line-spaced survey by taking even and odd line subsets from the current survey. It has already been noted that the most diagnostic match of measured and computed data is on one specific flightline across the centre of the anomaly (line 100660), that is included in only one of the alternate-line subsets.

Figure 6.45 shows TMI images generated by gridding the two separate 200 m spaced line sets, together with stacked profiles of the TMI data and of TMI forward computed from elliptic-section pipe models inverted to fit the individual datasets. The two TMI images appear quite similar, but with an apparent offset, because in either case gridding of the data does not displace the central peak of the anomaly far from an included flightline. For both datasets the stacked profiles of measured TMI and TMI forward-computed from the elliptic-section pipe model inversions show closer agreement than the corresponding match for the complete 100 m spaced set of flightlines. This is because the models have a less demanding task in fitting these sparser datasets. The model centre-points plotted in Fig. 6.45 are well clustered for inversion of different model geometries for each individual line dataset and are consistent between the two datasets. Figure 6.46 shows the model centre-point distribution in more detail. The points are all confined within a 100 m span of one flightline spacing (for the individual inversions this is equivalent to one-half of a 200 m flightline spacing) and are mostly clustered within a radius of 25 m about the best-estimate body centre. There is significantly larger scatter for the even line-number inversion models than for the odd line-number inversion models. The even line-number set includes the central flightline but has only that one line through the anomaly peak, whereas the odd line number subset has two (more marginal) lines through the anomaly peak.

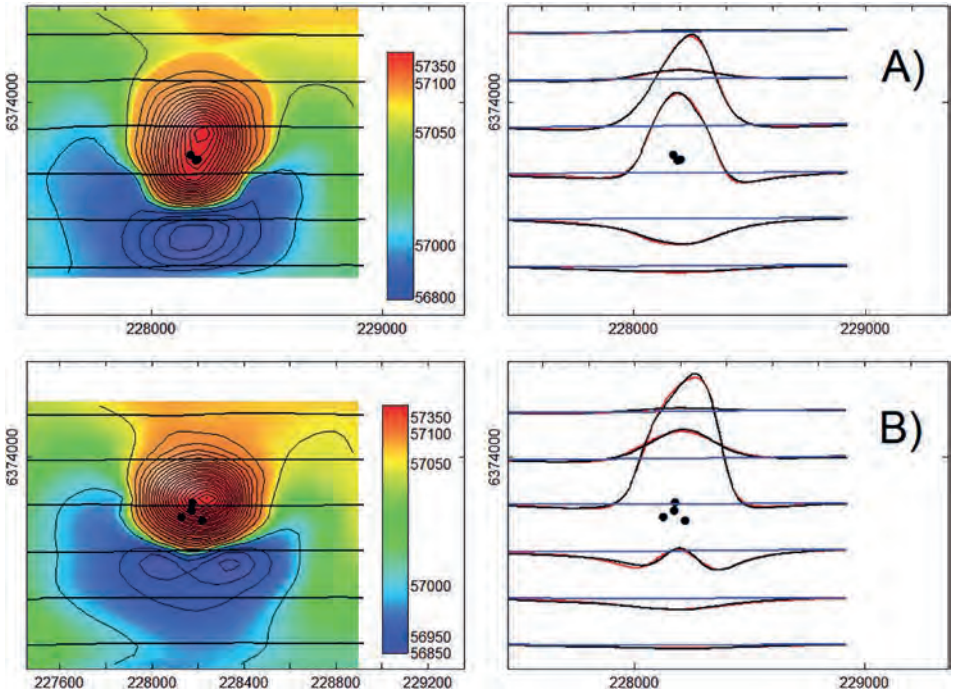

Fig. 6.45. TMI images and stacked profiles (black – measured, blue – interpreted regional, red – computed from elliptic pipe model on A) odd and B) even lines. Points mark centres of four inversion models (ellipsoid, tabular, circular and elliptic pipes).

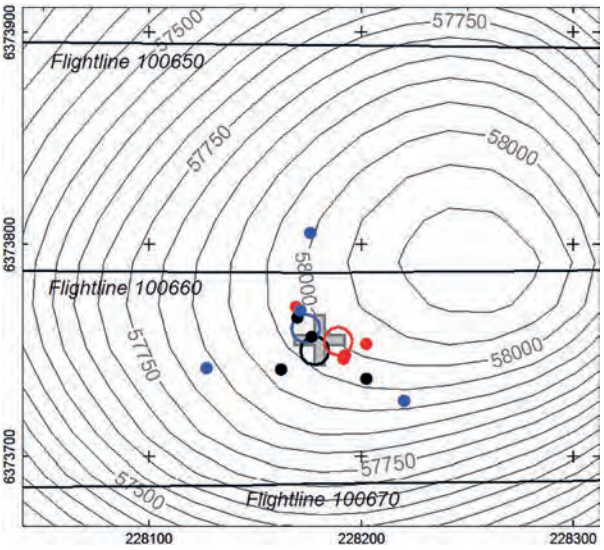

Fig. 6.46. Best inversion model centres from inversion of all lines (black points), odd-number lines (red points), even-number lines (blue points), with respective mean centres (open circles), global mean (grey cross), flightlines and TMI contours.

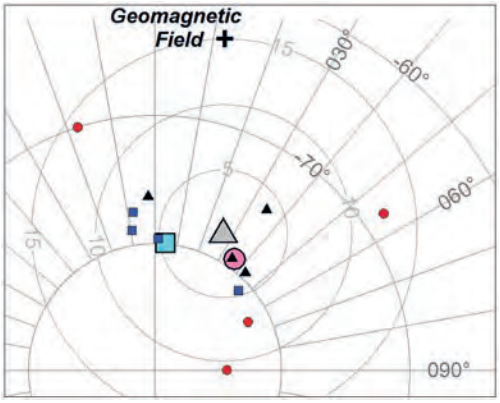

Fig. 6.47. Stereonet plot of model magnetisation directions from inversion of all lines (triangles), odd-number lines (red circles), and even-number lines (blue squares) with contours of rotation from the best direction (degrees).

Magnetisation directions recovered from the different model geometry inversions of the individual line datasets are plotted in Fig. 6.47. The different geometry inversions of the complete (100 m line-spaced) dataset cluster within 4° of the population best direction. The mean directions from different geometry model inversions of the individual line datasets are also within 4° of the best direction. Magnetisation directions of the different geometry inversions of the odd line number data are grouped within 5° of their mean direction, whereas directions for the even line number data are more scattered within 10°of their mean direction, consistent with the larger scatter of the model centre-points. Had the Rylstone survey been flown at 200 m line-spacing instead of 100 m, the best-estimated (multiple inversion) magnetisation direction should have been recovered within 5° of the best-estimated direction that was obtained from the 100 m line-spaced survey.

This study raises the question of what ground investigation would be required to validate the results. Many magnetic field anomalies in Australia are from sources buried beneath cover and no petrophysical or palaeomagnetic measurements are available unless there is oriented borehole core. The magnetic anomaly most regularly related to a measured magnetisation is the Black Hill Norite (Rajagopalan *et al*. 1993, 1995; Schmidt *et al.* 1993; Foss and McKenzie 2011) but those measurements were made on only a few samples from a single quarry outcrop which is not part of the source of the studied anomaly. The only case study I am aware of in which a model based on petrophysical measurements of susceptibility and remanent magnetisation has been quantitatively matched to its magnetic field anomaly is the Rover 3 anomaly studied by Austin and Foss (2014). That study used samples from only a single borehole, but the body is horizontally compact and the measured magnetisations assigned to horizontal units defined by abrupt and significant magnetisation contrasts produce an acceptable explanation of the measured anomaly. The volcanic unit causing the Rylstone anomaly is more likely to be irregularly inhomogeneous, with magnetisation intensities possibly varying by orders of magnitude over a range of scales, and with irregular and unpredictable distribution. The volume estimates for the magnetisation vary between 5×10^6 m^3 and 1.4×10^7 m^3, with horizontal widths between 350 and 450 m and depth extent from 70 to 160 m. Ground-truthing with direct palaeomagnetic measurements would depend on finding outcrop free from pervasive weathering and/or extensive lightning strike re-magnetisation. Even extensive suitable outcrop over the top of the body would provide a very limited sampling of the complete body. That would require oriented core from several boreholes to 100 or 200 m depth. The present inversion model volume and magnetisation estimates (Fig. 6.29) vary by more than a factor of 2, and models can be found to well match the anomaly with at least another variation factor of 2 to 5. To compare measured and inverted total magnetisations requires boreholes to intersect the base of magnetisation as well as effective constrains on the margins of the body. The concept of meaningfully constraining magnetisation models with petrophysics

measurements, as widely promoted in published literature, rarely take into account the variability of rock magnetisation and massively under-represents the challenge. Magnetisation is not a true bulk property of a rock – it depends completely on minerals that typically constitute only a few per cent of the rock, and the magnetisation of those minerals varies considerably with oxidation, iron/titanium ratios and grain size and shape. If measurements on core were to establish that there is high variability of magnetisation, then the homogeneous magnetisation intensity provided by an inversion model is only a bulk statistic for that rock unit and may not represent the true magnetisation at any point within it. The principal value of petrophysics measurements would be to relate magnetisation to mineralogy and geological processes in the history of the rock. Direct magnetisation measurements are also required to resolve the resultant magnetisation investigated in magnetic field analysis into its remanent and induced components.

6.9 CONCLUSIONS

In this chapter I provide empirical justification for recovery of magnetisation estimates from inversion of anomalies due to compact magnetisations, for which the maximum extension in any one direction is less than twice the closest point of measurement and/or computation of the magnetic field. The analytic capabilities of this study are provided by parametric inversion that permits isolation and study of single components of complex interactive problems. This study suggests that for isolated, well-defined anomalies due to compact sources of homogeneous magnetisation, uncertainty in source position, shape and plunge should not preclude recovering an estimate of that magnetisation direction from inversion of magnetic field data to within a range of 5° to 10°. For less favourable cases, however, errors in magnetisation direction of up to 15° may occur as a result of combined errors in estimation of source location and plunge.

The complexity of voxel inversion models does not clearly present the relationships established in this study, but the fundamental relationships between magnetisations and their magnetic fields apply to all inversion results provided magnetisations are compact and their fields are well isolated. If magnetisations are more distributed or more inhomogeneous than the discrete magnetisations represented by the parametric models of this study then the relationships degrade and inversion results lose significance. Existence of discrete features (sweet-spots) is essential for inversion to resolve distribution of magnetisation and its direction.

A comprehensive inversion study of Anomaly 276 in Rylstone, New South Wales has established the capability to recover estimates of magnetisation direction consistent to within 5° to 10°. The magnetisation direction of this source is not independently known so the magnetisation directions, while consistent are not presently proven correct. However, the sensitivity of estimated magnetisation direction to the distribution of magnetisation, its location and plunge are all shown to be in close agreement with relationships established from the synthetic data study. The best estimate of the maximum-extent to measurement-proximity ratio for the Rylstone anomaly is between 4.6:1 and 6.8:1. This is significantly larger than the value of 2 suggested as a conservative bound on compact sources. This promisingly suggests that compact source behaviour, favourable for estimation of source magnetisation direction, extends to a wide range of geological magnetisations and survey data. The magnetisation direction estimate is also shown to be stable through sub-sampling of the anomaly from the 100 m line spacing to 200 m.

ACKNOWLEDGEMENTS

I would like to thank the Geological Survey of New South Wales for supply of the data. All modelling and inversion studies were conducted with Tensor Research's ModelVision^{TM} software package.

REFERENCES

Austin JR, Foss CA (2014) The paradox of scale: reconciling magnetic anomalies with rock magnetic properties for cost-effective mineral exploration. *Journal of Applied Geophysics* **104**, 121–133. doi:10.1016/j.jappgeo.2014.02.018

Beiki M, Clark DA, Austin JR, Foss CA (2012) Estimating source location using normalized magnetic source strength calculated from magnetic gradient tensor data. *Geophysics* **77**, J23–J37. doi:10.1190/geo2011-0437.1

Clark DA (2014) Methods for determining remanent and total magnetisations of magnetic sources – a review. *Exploration Geophysics* **45**, 271–304. doi:10.1071/EG14013

Cooper GRJ (2014) Reducing the dependence of the analytic signal amplitude of aeromagnetic data on the source vector direction. *Geophysics* **79**, J55–J60. doi:10.1190/geo2013-0319.1

Dannemiller N, Li Y (2006) A new method for determination of magnetisation direction. *Geophysics* **71**, L69–L73. doi:10.1190/1.2356116

Dransfield M, Christensen A, Liu G (2003) Airborne vector magnetics mapping of remanently magnetized banded iron formations at Rocklea, Western Australia. *Exploration Geophysics* **34**, 93–96. doi:10.1071/EG03093

Encom Technology (1997) 'Interpretation of airborne geophysical data over the Rylstone Area.' The Coal and petroleum Geology Branch, The Geological Survey of New South Wales (unpublished), 23 pages.

Fedi M, Florio G, Rapolla A (1994) A method to estimate the total magnetisation direction from a distortion analysis of magnetic anomalies. *Geophysical Prospecting* **42**, 261–274. doi:10.1111/j.1365-2478.1994.tb00209.x

Foss CA (2006) 'Evaluation of strategies to manage remanent magnetisation effects in magnetic field inversion.' 76th Annual International Meeting, SEG, Expanded Abstracts, 938–942.

Foss CA (2017) Resultant-magnetisation based magnetic field interpretation. In *Proceedings of Exploration 17: Sixth Decennial International Conference on Mineral Exploration*. (Eds V Tschirhart, MD Thomas) pp. 637–648.

Foss CA, McKenzie KB (2011) Inversion of anomalies due to remanent magnetisation: an example from the Black Hill Norite of South Australia. *Australian Journal of Earth Sciences* **58**, 391–405. doi:10.1080/08120099.2011.581310

Fullagar PK, Pears GA (2015) 'Remanent magnetisation inversion.' 24th ASEG Conference, Extended Abstracts. doi:10.1071/ASEG2015ab188

Helbig K (1963) Some integrals of magnetic anomalies and their relation to the parameters of the disturbing body. *Zeitschrift für Geophysik* **29**, 83–96.

Keating P, Sailhac P (2004) Use of the analytic signal to identify magnetic anomalies due to kimberlite pipes. *Geophysics* **69**, 180–190. doi:10.1190/1.1649386

Lelièvre PG, Oldenburg DW (2009) A 3D total magnetisation inversion applicable when significant, complicated remanence is present. *Geophysics* **74**, L21–L30. doi:10.1190/1.3103249

Li X (2006) 'Understanding 3D analytical signal amplitude. *Geophysics* **71**, L13–L16. doi:10.1190/1.2184367

Paine J, Haederle M, Flis M (2001) Using transformed TMI data to invert for remanently magnetised bodies. *Exploration Geophysics* **32**, 238–242. doi:10.1071/EG01238

Phillips JD (2005) Can we estimate total magnetisation directions from aeromagnetic data using Helbig's integrals? *Earth, Planets, and Space* **57**, 681–689. doi:10.1186/BF03351848

Pratt DA, McKenzie KB, White TS (2014) Remote remanence determination (RRE). *Exploration Geophysics* **45**, 314–323. doi:10.1071/EG14031

Rajagopalan S, Schmidt PW, Clark DA (1993) Rock magnetism and geophysical interpretation of the Black Hill Norite, South Australia. *Exploration Geophysics* **24**, 209–212. doi:10.1071/EG993209

Rajagopalan S, Clark DA, Schmidt PW (1995) Magnetic mineralogy of the Black Hill Norite and its aeromagnetic and palaeomagnetic implications. *Exploration Geophysics* **26**, 215–220. doi:10.1071/EG995215

Roest WR, Pilkington M (1993) Identifying remanent magnetization effects in magnetic data. *Geophysics* **58**, 653–659. doi:10.1190/1.1443449

Schmidt PW, Clark DA (1998) The calculation of magnetic components and moments from TMI: a case study from the Tuckers igneous complex, Queensland. *Exploration Geophysics* **29**, 609–614.

Schmidt PW, Clark DA, Rajagopalan S (1993) An historical perspective of the Early Palaeozoic APWP of Gondwana: new results from the Early Ordovician Black Hill Norite of South Australia. *Exploration Geophysics* **24**, 257–262. doi:10.1071/EG993257

Yoo EK (1998) 'Western Coalfield Regional Geology (northern part) 1:100 000, 1st edition.' Geological Survey of New South Wales, Sydney.

Yoo EK, Tadros NZ, Bayly KW (2001) 'A compilation of the geology of the Western Coalfield.' Geological Survey of New South Wales, Report GS2001/204 (unpublished).